Kv7.2 Regulates the Function of Peripheral Sensory Neurons

Chih H. King,[1]* Eric Lancaster,[2] Daniela Salomon,[3] Elior Peles,[3] and Steven S. Scherer[2]

[1]Department of Neuroscience, The University of Pennsylvania School of Medicine, Philadelphia, Pennsylvania 19104
[2]Department of Neurology, The University of Pennsylvania School of Medicine, Philadelphia, Pennsylvania 19104
[3]Department of Molecular Cell Biology, Weizmann Institute of Science, Rehovot, Israel 76100

ABSTRACT

The Kv7 (KCNQ) family of voltage-gated K^+ channels regulates cellular excitability. The functional role of Kv7.2 has been hampered by the lack of a viable *Kcnq2*-null animal model. In this study, we generated homozygous *Kcnq2*-null sensory neurons using the Cre-Lox system; in these mice, Kv7.2 expression is absent in the peripheral sensory neurons, whereas the expression of other molecular components of nodes (including Kv7.3), paranodes, and juxtaparanodes is not altered. The conditional *Kcnq2*-null animals exhibit normal motor performance but have increased thermal hyperalgesia and mechanical allodynia. Whole-cell patch recording technique demonstrates that *Kcnq2*-null sensory neurons have increased excitability and reduced spike frequency adaptation. Taken together, our results suggest that the loss of Kv7.2 activity increases the excitability of primary sensory neurons. J. Comp. Neurol. 000:000–000, 2014.

INDEXING TERMS: KCNQ; M-current; dorsal root ganglion; nociceptors; Kv7

The Kv7 (KCNQ) family of K^+ channels is made up of five members, Kv7.1–Kv7.5 (Jentsch, 2000; Delmas and Brown, 2005; Brown and Passmore, 2009). Many peripheral nervous system (PNS) and central nervous system (CNS) neurons express Kv7.2, Kv7.3, and K7.5; in addition, Kv7.1 and Kv7.4 have recently been found in certain neuronal populations (Goldman et al., 2009; Heidenreich et al., 2011). Kv7.1 and Kv7.4 are prominently expressed in the cochlea, and Kv7.1 is expressed in the heart (Brown and Passmore, 2009). Kv7 channels contribute to the normal resting membrane potential and also form the noninactivating M-current, which is modulated by muscarinic agonists (Brown and Adams, 1980; Wang et al., 1998). Their importance in maintaining normal cellular excitability is demonstrated by the effects of dominant mutations of *KCNQ1*, *KCNQ2*, *KCNQ3*, and *KCNQ4* (all decrease the Kv7 current and cause hereditary diseases in a cell autonomous manner [Singh et al., 1998]) in the heart (*KCNQ1*), brain (*KCNQ2* and *KCNQ3*), and inner ear (*KCNQ1* and *KCNQ4*; Jentsch, 2000; Brown and Passmore, 2009). One *KCNQ2* mutation causes neuromyotonia (Dedek et al., 2001), a form of peripheral nerve hyperexcitability, which likely is the result of diminished Kv7.2 and Kv7.3 current at nodes of Ranvier, where Kv7.2 and Kv7.3 are localized (Devaux et al., 2004). A conserved ankyrin-G binding motif located at the C-termini mediates the localization of Kv7.2 and Kv7.3 at nodes and axon initial segments (AIS; Pan et al., 2006).

Previous investigations of the role of Kv7 in regulating neuronal excitability and nociceptive behaviors utilized pharmacological M-channel blockers and/or enhancers (Passmore et al., 2003; Yue and Yaari, 2004; Rivera-Arconada and Lopez-Garcia, 2006; Lang et al., 2008; Roza and Lopez-Garcia, 2008). Because homozygous *Kcnq2*-null mice die at birth from pulmonary atelectasis, investigators studied heterozygous *Kcnq2*-knockout mice (Watanabe et al., 2000; Yang et al., 2003; Otto et al., 2006; Tzingounis and Nicoll, 2008), *Kcnq3*-null mice (Tzingounis and Nicoll, 2008), or mice expressing a dominate-negative human *KCNQ2* mutation as a transgene (Peters et al., 2005). None of these studies, however, satisfy the need to develop an animal

Grant sponsor: National Institutes of Health; Grant number: R01NS43174; Grant sponsor: National Institutes of Neurological Diseases and Stroke; Grant number: NS50220; Grant sponsor: Binational Science Foundation.

*CORRESPONDENCE TO: Chih King, 450 Stemmler Hall, The University of Pennsylvania School of Medicine, Philadelphia, PA 19104.
E-mail: chk84@pitt.edu

Received September 30, 2013; Revised March 27, 2014;
Accepted March 28, 2014.
DOI 10.1002/cne.23595
Published online March 30, 2014 in Wiley Online Library (wileyonlinelibrary.com)

model with a complete absence of Kv7.2 expression. In addition, previous studies of heterozygous *Kcnq2*-knockout mice found that reduction of Kv7.2 expression involves a decreased seizure threshold (Watanabe et al., 2000; Yang et al., 2003).

The present study characterizes mice in which *Kcnq2* has been deleted in all somatic sensory neurons, using the Cre-Lox system (Sauer and Henderson, 1988; Nagy, 2000). These mice are viable, and their myelinated sensory axons have a normal ultrastructure and normal molecular composition of nodes (including Kv7.3), paranodes, and juxtaparanodes. *Kcnq2* mutant mice showed signs of thermal hyperalgesia and mechanical allodynia, and *Kcnq2*-null dorsal root ganglia (DRG) neurons showed increased excitability and reduced spike-frequency adaptation. Taken together, our results suggest that Kv7.2 regulates neuronal excitability and that a reduction of Kv7.2 expression could lead to altered nociception.

MATERIALS AND METHODS

All procedures involving rodents were approved by the Institutional Animal Care and Use Committee of the University of Pennsylvania. Except when specified, all chemicals were from Sigma (St. Louis, MO).

Generation of conditional *Kcnq2*-null mice

A floxed allele of *Kcnq2* was designed (see Fig. 1A) to delete exons 3–5; these correspond to 463 bp (amino acid 130–285) of mouse *Kcnq2* cDNA (GeneBank AF490773; Wen and Levitan, 2002); this deletion has been shown to result in a functional null allele (Watanabe et al., 2000). Two DNA fragments (EcoRV and XhoI) were cloned from R1 ES-cells genomic DNA and used to generate a targeting vector in which an FRT-neomycin-FRT-loxP cassette was inserted into a unique XhoI site, with flanking 7 kb and 3.4 kb of homologous genomic DNA. An additional loxP site was inserted in an EcoRI site just upstream of the third exon. The targeting vector also includes a diphtheria toxin (DT) gene as a negative selection marker against ES clones that have randomly integrated the targeting vector. The linearized targeting vector was electroporated into R1 embryonic stem cells, selected with G418, and colonies were picked and analyzed by Southern blot. Positive ES cells were used to generate chimeras and then heterozygous mice (Gollan et al., 2003; Poliak et al., 2003). The presence of the targeted locus was confirmed by polymerase chain reaction (PCR) analysis of tail DNA. Heterozygous mice were first mated with mice carrying the FLP recombinase (129S4/SvJaeSor-Gt(ROSA)26Sortm1(FLP1)Dym/J, RRID:IMSR_JAX:003946; Farley et al., 2000), to remove the *Neo* cassette and to create a floxed *Kcnq2* allele.

We crossed mice expressing *Pax3-Cre* (RRID:IMSR_JAX:005549) with mice carrying the *Rosa26* reporter gene (RRID:IMSR_JAX:003504). We examined X-gal expression in the brains, spinal cords, and lumbar DRG of three *Pax3-Cre*-positive//*Rosa26* mice and three *Pax3-Cre*-negative//*Rosa26* littermates, all 1-month-old, as previously described (Feltri et al., 1992; Arroyo et al., 1998). The mice were perfused with 0.5% glutaraldehyde in 0.1 M phosphate buffer (PB; pH 7.4); their cerebra, cerebelli, and spinal cords were dissected and cut into slabs with a razor blade; and the resulting sections along with L4 and L5 DRG were fixed for 3 hours at 4°C, stained in X-gal (Roche Diagnostics, Indianapolis, IN) at 37°C for 24–48 hours, rinsed in 0.1 M PB, then refixed in 3% glutaraldehyde (in 0.1 M PB) at 4°C overnight. The samples were photographed with a Nikon Coolpix 5000 camera mounted on a Leica MZ16 FA stereomicroscope. The DRG were osmicated, dehydrated, and embedded with the Embed 812 kit (EMS). Semithin sections (1 μm thick) were photographed with a cooled Hamamatsu camera mounted on a Leica DMR light microscope.

Kcnq2 was deleted in sensory axons by crossing with mice that were heterozygous for both the floxed *Kcnq2* allele and *Pax3-Cre* ($Kcnq2^{f/+}$//*Pax3-Cre*). We chose this approach because it generates relatively more mice of the desired genotype, and homozygous *Pax3-Cre* mice fail to develop past E18.5 according to Jackson Laboratory. All offspring were genotyped by PCR. Tail DNA was digested with DirectPCR (Viagen) and proteinase K overnight at 55°C and heated to 85°C for 45 minutes to denature proteinase K, and then PCRs were then performed with REDTaq ReadyMix PCR mix, following the manufacturer's protocol in a Bio-Rad DNA Engine Peltier thermal cycler. Three primers were used together: KCNQ2A (GGGGCAGTTGTCTAACCCTC), KCNQ2C (TATGTGGTGCTCCCCAGAAG), and KCNQ2E (GGGAGGCTC TAGTGTCAGTG; see Fig, 1B). After amplification, samples were separated in 1.5% agarose (GeneMate) gel in 1× TBS at 125 V for 1 hour. To detect the presence of *Pax3-Cre* in the control littermates ($Kcnq2^{+/+}$), three primers were used together: oIMR6977 (CTGCACTCAAGGGACTC CTC), oIMR6978 (GTGAAGGCGAGACGAAAAAG), and oIMR9074 (AGGCAAATTTTGGTGTACGG), following instruction provided by Jackson Laboratory.

Anatomical studies

One-month-old *Kcnq2*-mutant mice of either sex ($Kcnq2^{fl/fl}$//*Pax3-Cre*; n = 3) and their control littermates ($Kcnq2^{+/+}$//*Pax3-Cre*; n = 3) were anesthetized with ketamine/xylazine mix and killed by decapitation.

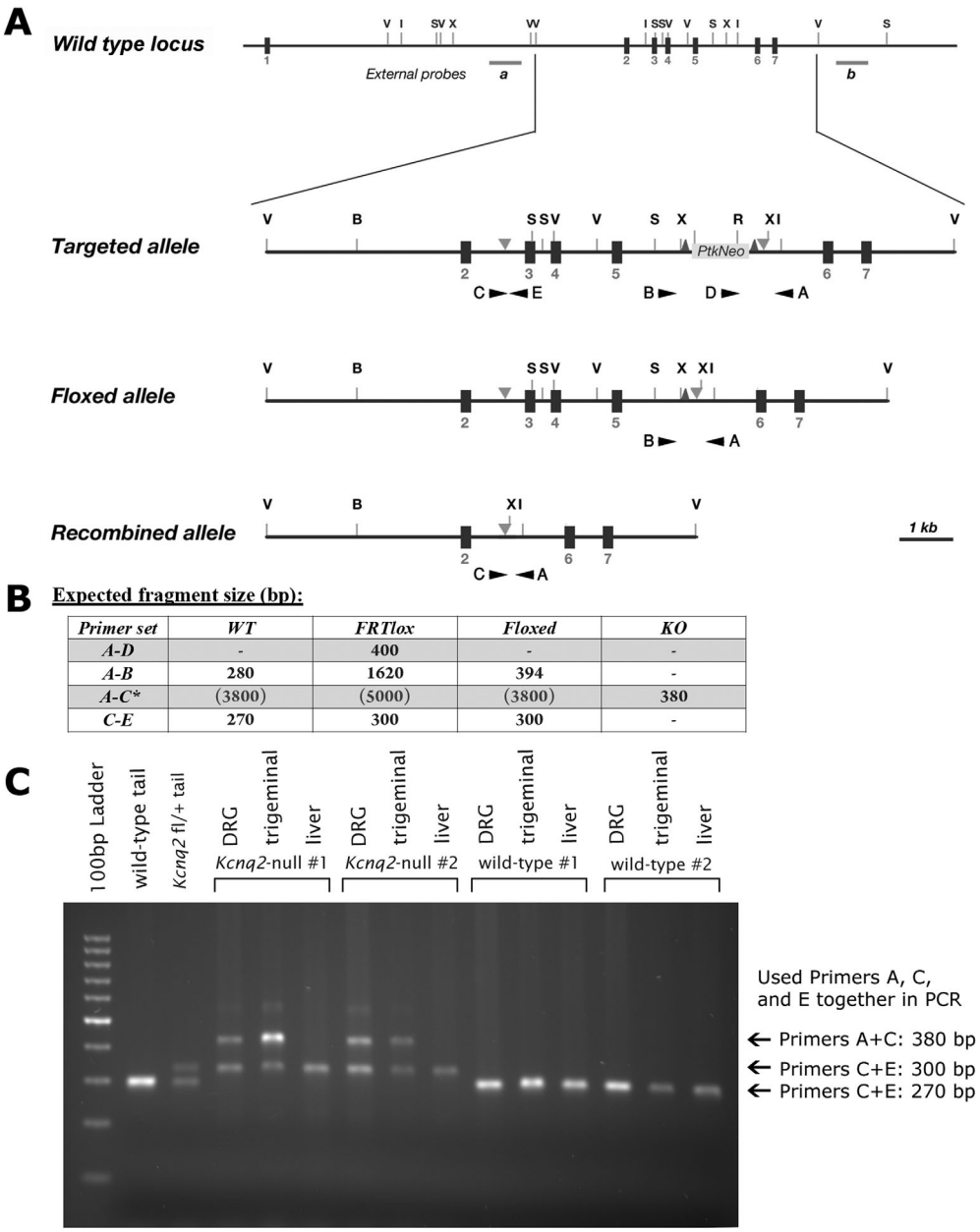

Primer set	WT	FRTlox	Floxed	KO
A-D	-	400	-	-
A-B	280	1620	394	-
A-C*	(3800)	(5000)	(3800)	380
C-E	270	300	300	-

Figure 1. Targeting strategy to generate an inducible deletion allele of *Kcnq2*. **A** shows the genomic arrangement of the first seven exons of wild-type *Kcnq2*. The external probes a and b are indicated as horizontal lines. The targeted allele contains two *loxP* sites (triangles facing downward) before the third and after the fifth exons. A cassette containing a *neo* gene under the herpes simplex *Tk* promoter (*PtkNeo*; boxed), flanked by two FRT sites (triangles facing upward) is inserted in a unique XhoI site in the intron between the fifth and the sixth exons. The targeting vector (not shown) is the same as the pictured targeted allele except that it includes a diphtheria toxin (DT) gene as a negative selection marker after the last EcoRV site. Mice carrying the floxed allele were obtained after the removal of the *PtkNeo* cassette by mating the targeted mice with a general FRT-deleter strain. The recombined allele lacks exons 3–5 and is generated after Cre-mediated deletion. **B** shows the expected sizes of the amplified DNA with the different primer pairs. **C** shows the PCR results of DNA isolated from DRG, trigeminal ganglia, and liver of *Kcnq2*-null mice and their control littermates, along with tail DNA from control and heterozygous floxed *Kcnq2* mice ($Kcnq2^{fl/+}$). Samples were subjected to PCR with the indicated primers, and the reaction products were separated by gel electrophoresis. An ~270-bp band, corresponding to the predicted size of wild-type *Kcnq2* allele, was detected in both tail samples as well as in all of the samples from the control littermates. An ~300-bp band, corresponding to the predicted size of the floxed *Kcnq2* allele, was detected in the heterozygous tail as well as in all of the *Kcnq2*-null samples. An ~380-bp band, corresponding to the predicted size of the recombined *Kcnq2* allele, was detected in both the DRG and the trigeminal ganglia of the *Kcnq2*-null mice but not in their liver.

TABLE 1.
List of Primary Antibodies Used

Name	Manufacturer	Dilution	Species	Type	Immunogen
KCNQ2N	A gift from Dr. Edward Cooper	1:200	Rabbit	Polyclonal	Human KCNQ2 N-terminus residues 13–37 (GEKKLKVGFVGLDPGAPDSTRDC)
KCNQ3C	A gift from Dr. Edward Cooper	1:200	Rabbit	Polyclonal	Human KCNQ3 C-terminus residues 578–604 (STPKHKKSQKGSAFTFPSQQSPRNEPYc)
KCNQ5	Chemicon; AB5599	1:1,000	Rabbit	Polyclonal	KCNQ5 N-terminus (M1-R88:GAAGLWVRSGAAAAAGAGGGRPGSGMKD VESGRGRVLLNSAAARGDGLLLLGTRAAALGGGGGG LRESRRGKQGARMSLLGK)
panNav	Sigma; clone K58/35 (S8809)	1:250	Mouse	Monoclonal	CTEEQKKYYNAMKKLGSKK from the intracellular III–IV loop of Na^+ channels
Kv1.1	NeuroMab; clone K20/78	1:250	Mouse	Monoclonal	Rat Kv1.1 amino acids 458–476 (CEEDMNNSIAHYRQANIRTG)
Caspr	A gift from Dr. Elior Peles; clone 275	1:100	Mouse	Monoclonal	Contained within extracellular domain of human Caspr (amino acids 1–1282)

Sciatic nerves, DRG (from L4–L6 spinal levels) with the ventral and dorsal roots attached, and femoral nerves (motor and sensory branches separately) were dissected and quickly embedded in OCT mounting media cooled in an acetone/dry ice slurry. The sciatic and femoral nerve fibers were teased apart with fine needles, mounted on SuperFrost Plus glass slides (Fisher Scientific, Pittsburgh, PA), dried overnight, and stored at −20°C. Ten-micromerter-thick cryostat sections were thaw-mounted onto SuperFrost slides and stored at −20°C. Teased fibers and OCT sections were immersed in −20°C acetone for 10 minutes, rinsed in Tris-buffered saline (TBS; pH 7.4), blocked at room temperature for 1 hour in TBS containing 5% fish skin gelatin and 0.5% Triton X-100, and incubated overnight at 4°C with various combinations of primary antibodies diluted in blocking solution. The slides were washed with TBS, incubated with the appropriate FITC- and TRITC-conjugated donkey cross-affinity-purified secondary antibodies (Jackson Immunoresearch, West Grove, PA; 1:200) at room temperature for 1 hour, washed with TBS, counterstained with 4′,6-diamidino-2-phenylindole dihydrochloride (DAPI; Invitrogen, Carlsbad, CA), mounted with Vectashield (Vector Laboratories, Burlingame, CA), and then examined with a Leica DMR light microscope with a cooled Hamamatsu camera under the control of Openlab software (PerkinElmer, http://www.perkinelmer.com/pages/020/cellularimaging/products/openlab.xhtml, RRID:rid_000096).

To analyze the structure of myelinated axons, 1-month-old *Kcnq2* mutant mice of either sex (*Kcnq2*$^{fl/fl}$*//Pax3-Cre*; n = 3) and littermates controls (*Kcnq2*$^{+/+}$*//Pax3-Cre*; n = 3) were perfused with 0.9% NaCl, followed by fixative (2% glutaraldehyde/2% paraformaldehyde in 0.1 M PB) for 10 minutes; then, the femoral sensory and motor branches as well as the L4 and L5 DRG were dissected, fixed for 4 hours at 4°C, osmicated, dehydrated, and embedded with the Embed 812 kit. Semithin (1 μm) sections were stained with toluidine blue and examined as described above; thin (80 nm thick) sections were stained with lead citrate and examined with a JEM-1010 transmission electron microscope (JEOL USA) outfitted with a digital camera.

Antibody characterization

See Table 1 for a summary of all primary antibodies used. The KCNQ2N antiserum (Dr. Edward Cooper; catalog No. KCNQ2N, RRID:AB_2312342) stained nodes and AISs of teased nerve fibers in a pattern identical to that previously shown (Devaux et al., 2004; Pan et al., 2006) and is directed against residues 13–37 (GEKKLKVGFVGLDPGAPDSTRDC) from the intracellular terminal region of human KCNQ2 (Cooper et al. 2001). The KCNQ3C antiserum (Dr. Edward Cooper; catalog No. KCNQ3C, RRID:AB_2312343), which detects residues 578–604 (STPKHKKSQKGSAFTFPSQQSPRNEPYc) of human KCNQ3 (Pan et al. 2006), also stained nodes in a pattern identical to that previously described (Pan et al., 2006). To ascertain the specificity of the Kv7.2 antisera, Hela cells were transiently transfected with the cDNA encoding human Kv7.2 or Kv7.3 (kindly provided by Dr. Edward Cooper) using the Lipofectamine 2000 (Invitrogen) method as previously described (Rasmussen et al., 2007) and immunostained 1 day post-transfection with the Kv7.2 and Kv7.3 antisera. The KCNQ2N antiserum positively stained Hela cells that were transiently transfected with the Kv7.2 cDNA but did not stain Hela cells transfected with Kv7.3 cDNA; the KCNQ3C positively stained transfected Hela cells expressing Kv7.3 but did not label transfected cells expressing Kv7.2 (data not shown).

The sequences of immunogen targeted by the KCNQ5 antiserum (Millipore Chemicon/Upstate/Linco; catalog No. AB5599, RRID:AB_210806) are a stretch of 88 amino acids from the N-terminal sequence of KCNQ5 (M1-R88:GAAGLWVRSGAAAAAGAGGGRPGSGMK DVESGRGRVLLNSAAARGDGLLLLGTRAAALGGGGGGLRES RRGKQGARMSLLGK) and were ascertained from both the manufacturer and from Caminos et al. (2007). The antiserum was able to label positively Hela cells transfected by the Kv7.5 cDNA (kindly provided by Dr. Thomas Jentsch) but did not label Hela cells transfected by the Kv7.2 cDNA (data not shown).

The mouse panNav monoclonal antiserum (Sigma-Aldrich; catalog No. S8809, RRID:AB_477552) targets multiple voltage-gated Na^+ channels and detects immunogen (CTEEQKKYYNAMKKLGSKK) from the intracellular III–IV loop of Na^+ channels (Rasband et al., 1999). Its specificity was confirmed by Western blotting of rat brain extracts recognizing a 260-kDa protein (manufacturer's technical information) and has previously been shown to stain specifically the AISs and nodes of a wide range of nervous tissues (Rasband et al., 1999; Devaux et al., 2004; Pan et al., 2006); in our stainings it recognized the nodes of both rat and mouse sciatic nerves, as expected.

The mouse monoclocal Kv1.1 antiserum (NeuroMab; catalog No. K20/78, RRID:AB_2312366) was prepared against a synthetic peptide representing amino acids 458–476 (CEEDMNNSIAHYRQANIRTG) of rat Kv1.1 (Rasband et al., 1998). Our Western blot analysis showed a strong band at about 85 kDa and a weaker band at about 65 kDa, identical to the information provided by the manufactuer (data not shown). In our staining it labeled the juxtaparanodal component of myelinated axons, as had been demonstrated previously (Rasband et al., 2001).

The mouse monoclonal contactin-associated protein (Caspr) antiserum (Peles et al., 1997; catalog No. contactin-associated protein [Caspr], RRID:AB_2311776) was generated by Dr. Poliak by immunizing mice with a fusion protein composed of the extracellular domain of human Caspr (amino acids 1–1282; Peles et al., 1997) fused to the Fc region of human immunoglobulin G and stained a single band of 180 kD molecular weight on Western blot (Poliak et al., 1999), In our staining it recognized the paranodes of mouse sciatic nerve, identical to previous descriptions (Poliak et al., 1999, 2003; Ogawa et al., 2010).

Behavioral testing

Three-month-old *Kcnq2* mutant mice (*Kcnq2*$^{fl/fl}$*//Pax3-Cre*; five males and four females) and their littermates (*Kcnq2*$^{+/+}$*//Pax3-Cre*; five males and four females), derived from three litters, were studied. Mechanical allodynia was measured using Chaplan's up-and-down threshold method (Chaplan et al., 1994; Hubbard and Winkelstein, 2005; Lee et al., 2008; Quinn et al., 2010). Mice were confined in a plexiglass enclosure placed on a wire-mesh platform and allowed to acclimate for at least 30 minutes before each test. Three rounds of testing were performed over 3 consecutive days, with each round comprising five stimulations of either the right or the left midplantar hindpaw in a random order, with a series of ascending von Frey filament strengths (0.4, 0.6, 1.0, 1.4, and 2.0 g; Stoelting Co., Wood Dale, IL) held perpendicular for 6–8 seconds against the skin with enough force to cause slightly buckling. A positive response is recorded for sharp paw withdrawal or if immediate flinching was observed upon removal of filament. Ambulation was considered an ambiguous response, and in such cases the stimulus was repeated. If two consecutive filament strengths elicited a withdrawal response, the lower of the two filament strengths was recorded as the threshold. Any mouse that failed to display a response with the highest filament strength was recorded as having a threshold of 2.0 g. Testing in the opposite direction (descending filament strength) was also performed during each round to confirm the withdrawal threshold. The average threshold of the three rounds was recorded for each mouse.

The thermal nociceptive response was assessed using a paw thermal stimulator system (UARDG, University of California San Diego; otherwise referred to as Hargreaves apparatus) as previously described (Hargreaves et al., 1988; Dirig et al., 1997). Four rounds were performed over 4 consecutive days. Briefly, the mice were allowed to acclimate on the glass plate of the apparatus (maintained at 30°C) for at least 30 minutes; then, either the left or the right midplantar hindpaw was randomly heated with a thermocouple set at 5 amperes. A timer is automatically started with the thermal source, and response latency is defined as the time required for the hindpaw to show an abrupt withdrawal (maximum 20 seconds). Paw withdrawal is automatically detected by an array of photodiode motion sensors mounted on the stimulus tower that stops the timer and terminates the stimulus. Stimulus current is monitored continuously. Six trials were performed during each round, with a minimum of 5 minutes between each trial to allow the hindpaws to return to normothermic baseline (Dirig et al., 1997). The average threshold of the four rounds was recorded for each mouse.

Motor function was measured with a rotarod apparatus (Ugo Basile, Stoelting Co.) as previously described (Wood et al., 2005; Oliveira et al., 2006). Briefly, the

rotarod has a 3-cm-diameter rotating rod raised 16 cm above a platform and divided into five sections for testing multiple mice simultaneously. Mice were acclimated on the first day by allowing them to run on the rotarod with the slowest rotation speed. Three rounds of testing were performed during the 3 subsequent days, with three trials during each round. For each trial, mice were placed on the rotarod, and the rotation speed was gradually increased from 4 to 40 rpm over the course of 5 minutes. Each trial ended when mice fell off (maximum 300 seconds), and the latency to fall was recorded for each trial. The test was considered valid if mice ran forward on the rotarod for at least 10 seconds. Mice were given 1 hour of rest between each trial. The average time to fall for each mouse was used as the outcome.

Whole-cell patch recording

DRG neurons were dissected and cultured from 3-month-old *Kcnq2* mutant mice of either sex (*Kcnq2*$^{fl/fl}$*//Pax3-Cre*; n = 5) and their littermate controls (*Kcnq2*$^{+/+}$*//Pax3-Cre*; n = 5) from two litters, as previously described (Malin et al., 2007). Lumbar DRGs were rapidly removed, transferred to ice-cold Ca^{2+}/Mg^{2+}-free HBSS (Gibco, Grand Island, NY), then incubated first in papain solution (60 U papain; Worthington, Columbus, OH), 3 μl saturated $NaHCO_3$, 1 mg L-cysteine free base, 1.5 ml Ca^{2+}/Mg^{2+}-free HBSS (Gibco) for 10 minutes at 37°C and then in collagenase/dispase solution (0.1 U/ml collagenase 0.8 U/ml dispase [Roche], 3 ml Ca^{2+}/Mg^{2+}-free HBSS) for 1 hour at 37°C. Neurons were dissociated by trituration using fire-polished glass Pasteur pipettes, suspended in F12 medium (Gibco) containing 10% FCS (Invitrogen) and 1% penicillin/streptomycin (Invitrogen), then plated onto laminin/poly-D-lysine (Beckton Dickson)-coated coverslips (Fisher). DRG neurons adhered to coverslips and were maintained in culture for 12–48 hours after plating at 37°C prior to recording.

Whole cell patch-clamp techniques (Hamill et al., 1981; Lancaster et al., 2001) were employed with an Axopatch 200B amplifier and Axon Instruments pClamp 9 software (pClamp; http://www.moleculardevices.com/products/software/pclamp.html, RRID:rid_000085). Patch pipettes (1–4 MΩ) were fabricated from glass capillaries (MTW150F-4; World Precision Instruments, Sarasota, FL). Pipettes were filled with a variant of a solution described previously (Ikeda et al., 1986), with a composition (in mM) of 140 KCl, 2 MgATP, 10 *N*-[2-hydroxyethyl] piperazine-*N*9-[2-ethanesulfonic acid] (HEPES), 11 ethylene glycolbis(b-aminoethyl ether)-*N*,*N*,*N*9,*N*9-tetraacetic acid (EGTA), and 2 $CaCl_2$, titrated to pH 7.3 with KOH and to 314 mOsm with sucrose. Pipette voltage offset was neutralized prior to the formation of a gigaseal. Membrane input resistance (R_{in}), series resistance (R_s), and capacitance (C_m) were determined from current transients elicited by 5-mV depolarizing steps from a holding potential of −60 mV, delivered using the Membrane Test application of pClamp9. Criteria for cell inclusion in the study were as follows: $R_s \leq 10$ MΩ, $R_{in} \geq 100$ MΩ, and stable recording during the entire experiment. Coverslips were superfused (2–4 ml/minute) continuously during recording at 34–36°C extracellular solution (composition in mM: 10 glucose, 140 NaCl, 3 KCl, 0.6 $MgCl_2$, 2.5 $CaCl_2$, 10 HEPES, titrated to pH 7.4 with Tris base to 325 mOsm with sucrose if needed). Tetraethylammonium (TEA) was fully dissolved in the extracellular solution prior to application; 3 mM TEA was applied for at least 2 minutes before determining its effects on membrane properties. To prevent bias in cell selection or analysis, the electrophysiologist was blinded to genotypes of the cells (control vs. *Kcnq2*-null) during the experiments and measurements of cell properties. In total 25 neurons from mutant mice and 25 neurons from control littermates were recorded and analyzed.

Statistical analysis

Other than the following exceptions, all comparisons between two samples were explored by unpaired two-samples Student's *t*-test, with equal variance first established with the equality of variance test. All statistical tests were performed in SAS 9.2 (Statistical Analysis System, http://www.sas.com/en_us/software/sas9.html, RRID:nif-0000–31484), with all data given as mean ± standard error of the mean (SEM). Comparison of Kv7.2- and Kv7.3-positive nodes in different peripheral nerves was tested with two-way ANOVA; motor function results over the course of nine sessions were analyzed with repeated-measures ANOVA; two-way repeated-measures ANOVA was used to compare mutant and control neurons before and after 3 mM TEA across multiple rheobases, followed by the Tukey test to identify specific significant differences. The minimum a priori criteria for statistical significance is $P < 0.05$.

RESULTS

Generation of conditional *Kcnq2*-null mice

We generated sensory neurons lacking *Kcnq2* expression by using the Cre-Lox system (Sauer and Henderson, 1988; Nagy, 2000). Mice containing a floxed allele of *Kcnq2* (Fig. 1A) were crossed with mice expressing a *Pax3-Cre* transgene, which is expressed by cells derived from the neural crest (Li et al., 2000). To determine whether *Pax3-Cre* deleted exons 3–5 of *Kcnq2*, we

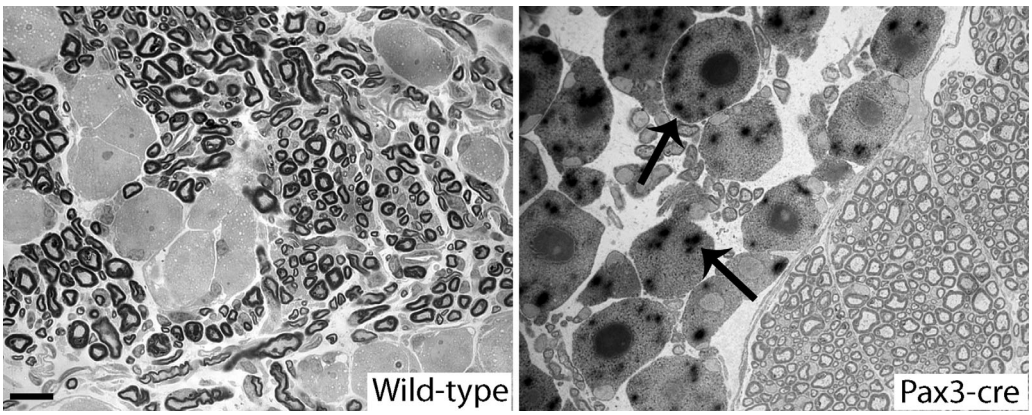

Figure 2. Sensory neurons expressed *Pax3-Cre*. Digital images of 1-μm-thick epoxy sections of DRG neurons from *Pax3-Cre*-positive (n = 3) and -negative (n = 3) mice that also expressed the *Rosa26* reporter gene. The DRGs had been labeled with X-gal. Almost all of the *Pax3-Cre*-positive neurons showed X-gal staining (two are indicated with arrows), whereas none of the neurons from control mice showed X-gal staining. Scale bar = 20 μm.

examined three *Kcnq2*$^{fl/fl}$//*Pax3-Cre* mice by amplifying genomic DNA with PCR and appropriate primers (Fig. 1A,B). As shown in Figure 1C, although both the floxed and the recombined *Kcnq2* alleles were detected in the DRG and trigeminal ganglia, only the floxed allele was detected in the liver, indicating that the *Kcnq2* allele was being selectively deleted in neural-crest-derived tissues.

We examined the expression of the *Pax3-Cre* by crossing the mice with *Rosa26 lacZ* reporter mice, in which Cre removes a floxed stop cassette so that *lacZ* is expressed (Soriano, 1999). Using litters that contained mice of the informative genotypes, we stained the brain, spinal cord, and DRG for β-galactoside activity with X-gal as the chromogen. None of the samples taken from the control animals showed X-gal staining, whereas, in *Pax3-Cre*//*Rosa26* mice, there was robust staining in much of the cerebellum, regions of the cerebrum (including the cortex and the thalamus), the dorsal part of the spinal cord (including the dorsal roots), and the DRG (data not shown). The ventral part of the spinal cord and the ventral roots were unstained, suggesting that motor neurons do not express *Pax3-Cre*. Semithin sections demonstrated that virtually all DRG neurons from the *Pax3-Cre*-positive mice showed X-gal staining (Fig. 2), indicating that DRG neurons and/or their embryonic precursors express *Pax3-Cre*.

Primary sensory neurons in conditional *Kcnq2*-null mice lacked Kv7.2

To determine whether *Pax3-Cre* resulted in the loss of Kv7.2 expression in sensory neurons, we examined three mutants (*Kcnq2*$^{fl/fl}$//*Pax3-Cre*) and three control littermates (*Kcnq2*$^{+/+}$//*Pax3-Cre*). We immunostained unfixed teased nerve fibers from femoral sensory and motor branches and from dorsal and ventral roots, as well as sections of the lumbar DRG, for Kv7.2 or Kv7.3, combined with a mouse monoclonal antibody against voltage-gated Na^+ channels (panNav). As shown in Figure 3, in the control mice, all nodes of Ranvier of both the motor and the sensory branches of the femoral nerve were Kv7.2 and panNav positive, agreeing with our previously published results (Devaux et al., 2004; Pan et al., 2006). In mutant animals, all nodes were panNav positive, but none of the nodes of the femoral sensory branch and only some nodes of the femoral motor branch were Kv7.2 positive. The lack of nodal staining of the *Kcnq2*-null sensory axons supports the specificity of the Kv7.2 antiserum, which also selectively labeled HeLa cells transiently transfected to express human Kv7.2 but did not label transfected cells expressing Kv7.3 (data not shown). Similarly, none of the nodes in the dorsal roots (which are purely sensory) and all of the nodes in the ventral roots (which are purely motor) were Kv7.2 positive (Fig. 4). Another Kv7.2 antiserum (provided by Dr. Jérôme Devaux) gave similar results (data not shown).

We also immunostained sections of lumbar DRG and trigeminal ganglia with the Kv7.2 antiserum. As shown in Figure 5, in control animals, the Kv7.2 antiserum labeled predominantly larger diameter DRG neurons (most of which were panNav negative), whereas the panNav antibody primarily labeled smaller diameter neurons. In contrast, for the mutants, we did not detect robust Kv7.2 staining in any neurons, and the panNav antibody retained its staining pattern. Notably, similar to the teased fibers, nodes in the *Kcnq2*-null DRG were

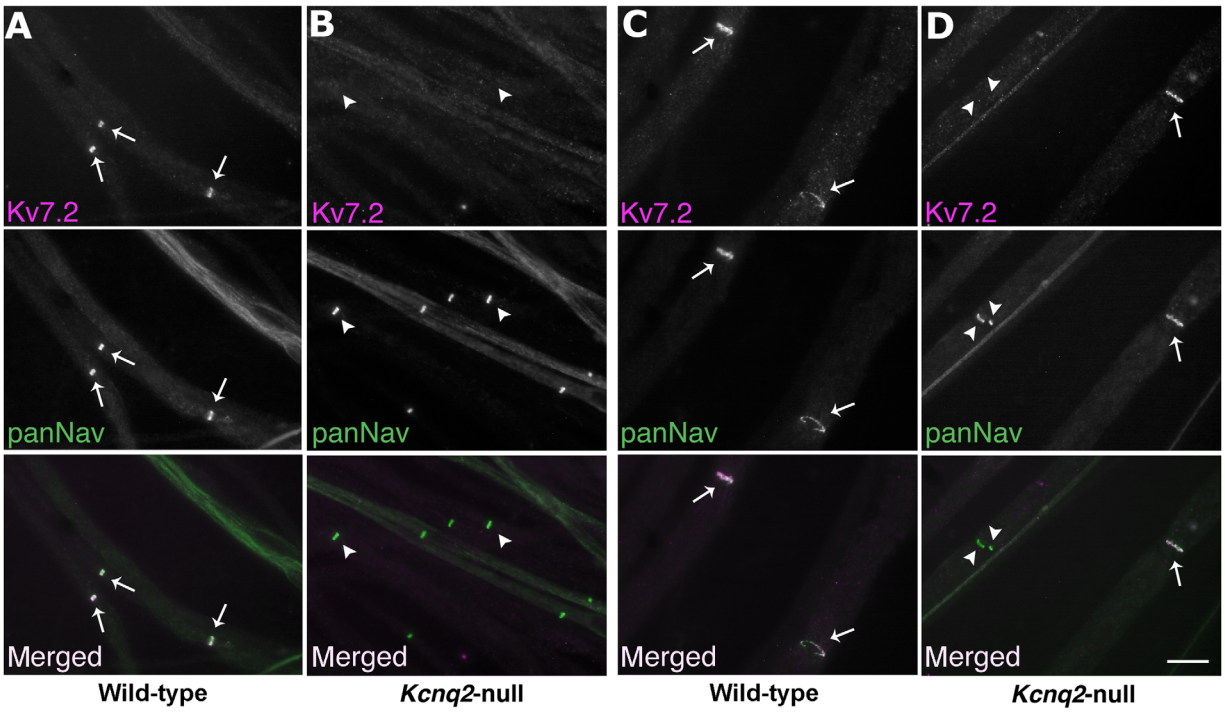

Figure 3. Selective loss of *Kcnq2* from the nodes of sensory axons. Digital images of unfixed teased fibers, double labeled for Kv7.2 (magenta) and voltage-gated sodium channels (panNav; green). In the femoral sensory branch (columns A and B), Kv7.2 is found at all nodes of Ranvier (arrows) in control animals but is not detected at any nodes (arrowheads) in *Kcnq2*-null animals. In the femoral motor branch (columns C and D), Kv7.2 is found at all nodes of Ranvier (arrows) in control animals but is not detected at some nodes (arrowheads) in *Kcnq2*-null animals. Scale bar = 10 μm.

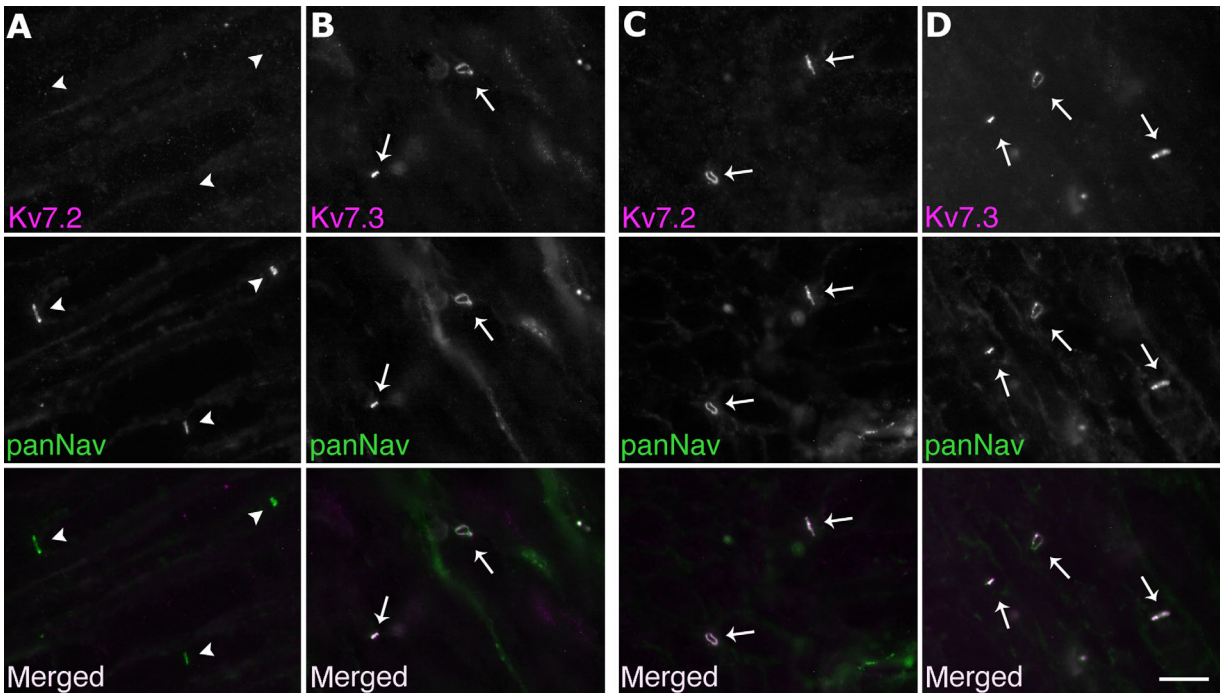

Figure 4. Selective loss of *Kcnq2* from the nodes of sensory axons. Digital images of unfixed mouse teased nerves, double labeled for either Kv7.2 or Kv7.3 (magenta) and panNav (green). In the dorsal roots of mutant animals (columns A and B), Kv7.2 is not detected at any node (arrowheads), whereas Kv7.3 is found at every node (arrows). In the ventral roots of mutant mice (columns C and D), note that all nodes are Kv7.2 and Kv7.3 positive (arrows). Scale bar = 10 μm.

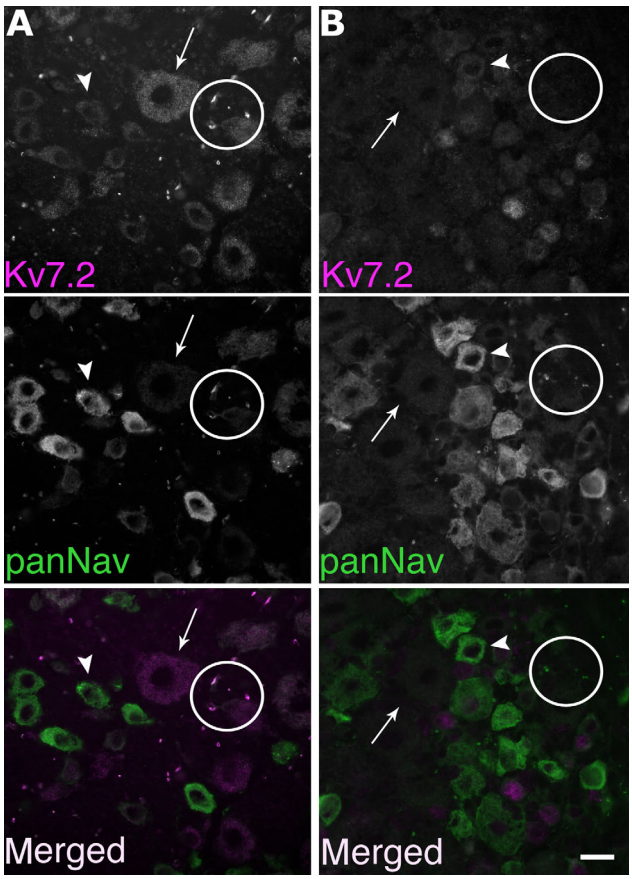

Figure 5. Primary sensory neurons of *Kcnq2*-null mice do not express Kv7.2. Images of unfixed sections of lumbar DRG, double labeled with a rabbit antiserum against Kv7.2 (magenta) and a panNav monoclonal antibody (green). In control DRG (column A), the Kv7.2 antiserum labels large-diameter neurons, one of which is indicated (arrow); these are relatively unlabeled by the panNav antibody. In contrast, in *Kcnq2*-null DRG (column B), the Kv7.2 antiserum does not label large neurons (arrow). In both control and *Kcnq2*-null DRG, the panNav monoclonal labels small neurons, two of which are indicated (arrowhead). In addition, all nodes of control neurons are double labeled by both Kv7.2 and panNav (some enclosed within a circle), whereas none of the nodes of mutant neurons is Kv7.2 positive. Scale bar = 20 μm.

Kv7.2 negative. We also found similar results in the trigeminal ganglia (data not shown), with a loss of Kv7.2 immunostaining in the neurons and nodes of mutant animals. Thus, we conclude that *Pax3-Cre* deleted *Kcnq2* from virtually all primary sensory neurons.

In vitro studies have shown that Kv7.2 and Kv7.3 can form heteromeric channels and that Kv7.2 increases cell membrane expression of Kv7.3 (Wang et al., 1998; Selyanko et al., 2001; Shah et al., 2002; Maljevic et al., 2003; Gomez-Posada et al., 2010). Because Kv7.2 and Kv7.3 are colocalized at nodes in vivo (Pan et al., 2006; Schwarz et al., 2006), we investigated whether nodal expression of Kv7.3 requires Kv7.2. As shown in Figures 4 and 6, all nodes of mutant mice showed robust Kv7.3 immunostaining, the femoral motor and sensory branches as well as the dorsal and ventral roots. Thus, nodal expression of Kv7.3 does not require Kv7.2.

To quantify these results, we calculated the proportion of Kv7.2- or Kv7.3-positive nodes in each of the four nerve branches (femoral sensory, femoral motor, ventral root, and dorsal root) among all panNav-positive nodes. As shown in Figure 7, the proportions of Kv7.2-positive nodes in the dorsal root (1.4% ± 0.06%), femoral sensory branch (0.48% ± 0.48%), and femoral motor branch (47% ± 1.6%) of the mutant animals were significantly less than in control littermates (99% ± 0.55%, 98% ± 0.53%, 96% ± 0.95%, respectively). As expected, the proportion of Kv7.2-positive nodes in the ventral root is not different between the mutants (99% ± 0.60%) and the controls (97% ± 0.41%), and the proportions of Kv7.3-positive nodes in all four nerve branches were found to be nearly 100% in both mutant and control mice.

We examined the structure of *Kcnq2*-null myelinated axons. Teased fibers from mutant sciatic nerves (in which approximately 20% of myelinated axons are motor and the remaining are sensory; Schmalbruch, 1986) were immunostained for Kv7.2 and panNav, Caspr, or Kv1.1. As shown in Figure 8, the localizations of selected nodal (panNav), paranodal (Caspr), and juxtaparanodal (Kv1.1) components were the same for myelinated axons from either Kv7.2-positive (motor axons) or Kv7.2-negative (sensory axons) nodes. The motor and sensory axons of the femoral nerves and dorsal roots of the mutant animals appeared normal in semithin cross-sections (data not shown). Longitudinal thin sections of femoral sensory nerves were visualized by electron microscopy. The paranodal loops, nodal microvilli, and nodal axolemma all appeared normal (data not shown).

Finally, because we had previously demonstrated that Remak fibers, but not nodes of Ranvier, express Kv7.5 (King and Scherer, 2012), we wished to determine whether this pattern of expression is retained in *Kcnq2*-mutant mice. As shown in Figure 9, in both the femoral sensory and femoral motor branches, Remak fibers of both control and mutant mice showed robust Kv7.5 immunostaining. Nodes were Kv7.5 negative, indicating that Kv7.3 forms homomeric channels in the *Kcnq2*-null axons.

Behavioral testing of mutant and control mice

We tested nine mutants ($Kcnq2^{fl/fl}$//*Pax3-Cre*) and nine control littermates ($Kcnq2^{+/+}$//*Pax3-Cre*) from three litters in a battery of tests. Mutant and control

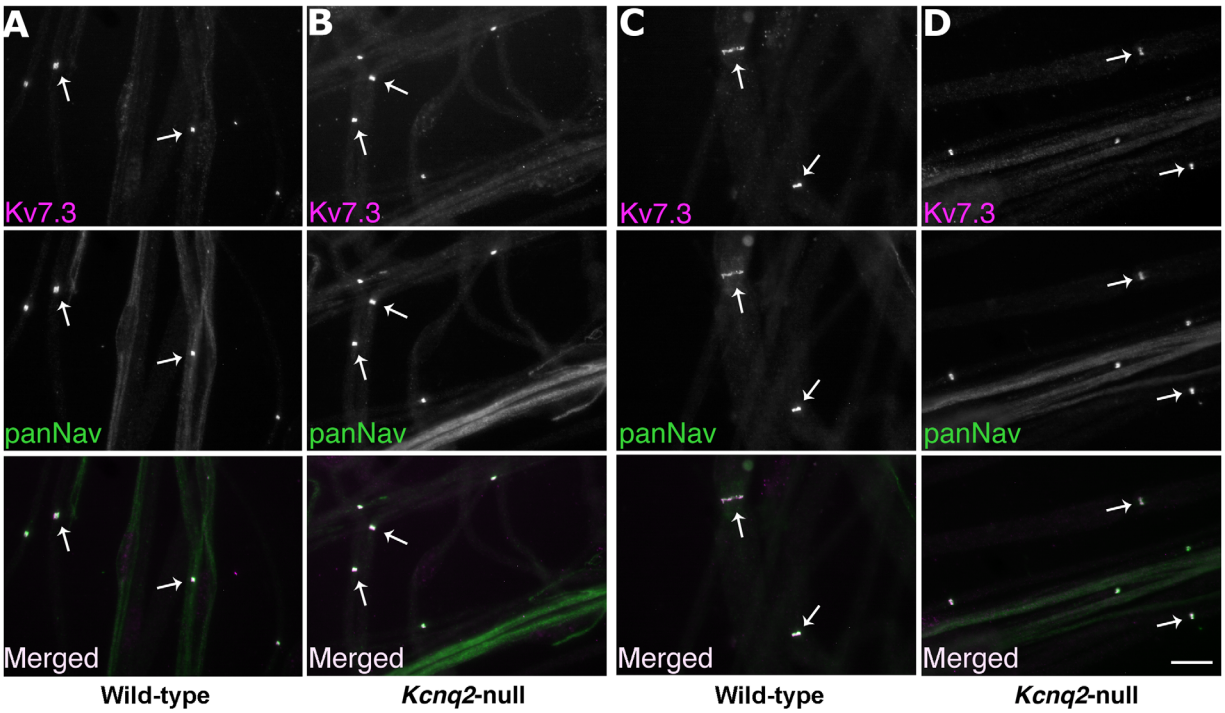

Figure 6. Kv7.3 is found at all nodes in *Kcnq2*-null mice. Digital images of unfixed mouse teased nerves, double labeled for Kv7.3 (magenta) and panNav (green). In the femoral sensory (columns A and B) and motor (columns C and D) branches of both mutant and control mice, all panNav-positive nodes are also Kv7.3 positive (arrows). Scale bar = 10 μm.

mice performed the rotarod test equally well (Fig. 10A) and showed similar performance improvement over the nine testing sessions across 3 consecutive days (data not shown). The average time to fall for all sessions was not statistically different between mutant (163 ± 13 seconds) and controls(170. ± 6.1 seconds) groups ($P = 0.62$). To determine whether mutant mice have altered thermal hyperalgesia, we measured the withdrawal latency from noxious thermal stimuli using the Hargreaves test over 4 consecutive days. As shown in Figure 10B, the mutant mice on average had significantly shorter withdrawal latency (3.7 ± 0.16 seconds) than did controls (4.3 ± 0.16 seconds; $P < 0.05$). To determine whether mutant mice have altered mechanical allodynia, we measured pain withdrawal threshold using von Frey filaments over 3 consecutive days. As shown in Figure 10C, the mutants had a significantly lower average withdrawal threshold (0.65 ± 0.07 g) compared with the controls (0.93 ± 0.09 g; $P < 0.05$). Taken together, our behavior tests suggest that the loss of Kv7.2 expression leads to increased thermal hyperalgesia and mechanical allodynia.

Electrophysiological studies of DRG neurons

We examined the electrophysiological characteristics of acutely isolated DRG neurons from the lumbar DRG from five mutants (*Kcnq2*$^{fl/fl}$//*Pax3-Cre*) and five controls (*Kcnq2*$^{+/+}$//*Pax3-Cre*) from two litters, using whole-cell patch-clamp recordings (Table 2). From each genotype, we recorded from 25 neurons of various sizes; the average cell size recorded from each genotype (as estimated from membrane capacitance) was not statistically different between the two groups (39 ± 3.3 pF vs. 45 ± 4.1 pF, respectively). The initial resting membrane potential was also not statistically different between the two groups (−58 ± 2.5 mV vs. −56 ± 1.6 mV, respectively).

To investigate the fast and slow afterhyperpolarization (AHP) properties, we elicited single action potential (AP) with brief (3 ms) depolarizing current steps and measured the peak undershoot (most negative potential during the AHP), as shown schematically in Figure 11A. Prior to applying TEA, the average fast AHP peak undershoot of mutant DRG neurons was 3 mV more negative than control neurons (−86 ± 0.97 mV vs. −83 ± 1.3 mV, respectively; $P < 0.05$). After applying 3 mM TEA, the fast AHP peak magnitudes were not significantly different between the mutant and the control neurons (−84 ± 1.2 mV vs. −82 ± 0.97 mV, respectively; $P = 0.24$; Fig. 11B). In contrast, prior to 3 mM TEA, the average slow AHP peak undershoot of mutant neurons was 6 mV more positive than that of control neurons (−68 ± 1.2 mV vs. −74 ± 1.9 mV, respectively; $P < 0.01$). After applying 3

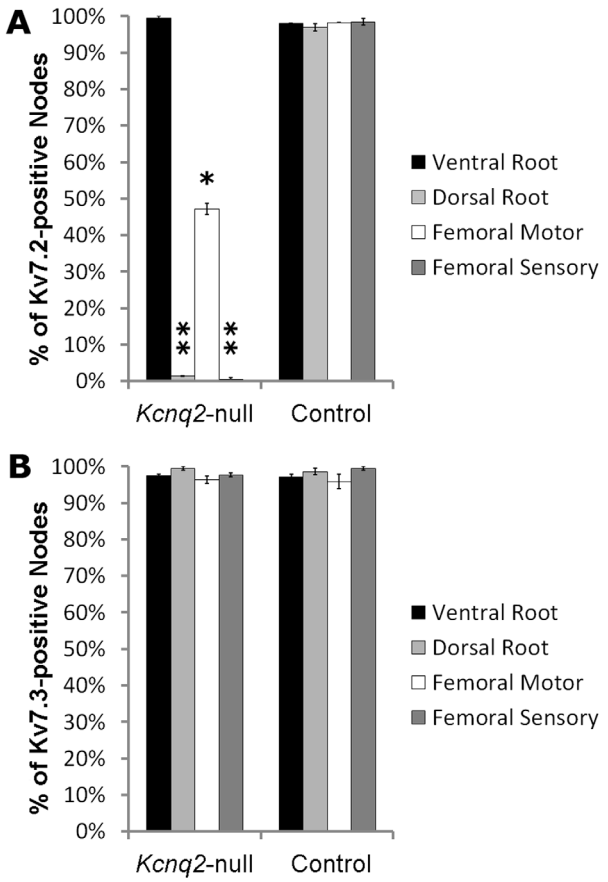

Figure 7. Selective loss of *Kcnq2*, but not *Kcnq3*, from the nodes of sensory axons. The bars represent average proportions of panNav-positive nodes that are Kv7.2 (**A**)- or Kv7.3 (**B**)-positive from the indicated source (n = 3 for all samples). Note that ~0% of nodes in the dorsal root and femoral sensory branch and 50% in the femoral motor branch were Kv7.2 positive. Error bars represent SEM. $*P < 0.05$, $**P < 0.01$ (two-way ANOVA).

mM TEA, the slow AHP peak undershoot of control neurons became 8 mV more positive (-66 ± 1.2 mV; $P < 0.01$), and the slow AHP peak undershoot of *Kcnq2*-null neurons did not change significantly (-67 ± 1.6 mV; Fig. 11C). Because 3 mM TEA should selectively block primarily the Kv7.2 homomers and Kv7.2/Kv7.3 heteromers but not Kv7.3 homomers (Wang et al., 1998; Hadley et al., 2000, 2003; Lerche et al., 2000), these results indicate that inhibiting Kv7.2 contributes to the decreased slow AHP peak undershoot observed in the mutant DRG neurons.

We examined the AP firing patterns and spike-frequency adaptation by injecting 500-ms depolarizing current steps into the DRG neurons. First, the threshold current (rheobase) for each neuron was determined using incremental (100 pA) 500-ms current steps (starting from 0.1 nA). Then we recorded the number of APs evoked by 500-ms depolarizing current steps of 1×, 2×, and 3× rheobase. To determine the responsiveness of DRG neurons to absolute (as opposed to relative threshold as described above) depolarizing stimuli, we also injected a series of 500-ms current steps from 0.4 nA to 3.6 nA (in increments of 0.4 nA). As shown in Figure 12, the *Kcnq2*-null neurons produced significantly more APs and exhibited less spike-frequency adaptation than did control neurons, and 3 mM TEA significantly increased the number of APs and decreased spike-frequency adaptation in control neurons but not in *Kcnq2*-null neurons (numbers of AP from each group – control neurons: 1× rheobase 2.1, 2× rheobase 5.8, 3× rheobase 8.04, absolute 15.6; *Kcnq2*-null neurons: 1× rheobase 2.9, 2× rheobase 11.2, 3× rheobase 17.44, absolute 24.4; two-way repeated-measures ANOVA). In addition, 3 mM TEA decreased the rheobase of control neurons by 49% (Table 2; 0.39 ± 0.07 nA from 0.77 ± 0.23 nA; $P < 0.05$), which is also statistically different from the value for mutant neurons after TEA (0.88 ± 0.19 nA; $P < 0.05$). In contrast, the rheobase of the mutant neurons was not affected by TEA (0.88 ± 0.19 nA from 0.81 ± 0.16 nA; $P = 0.78$). In summary, mutant DRG neurons displayed increased excitability and decreased spike-frequency adaptation, and this hyperexcitability could be replicated in control neurons by 3 mM TEA.

DISCUSSION

Deleting *Kcnq2* enabled us to investigate directly the role of Kv7.2 in sensory neurons. As expected, deleting Kv7.2 had no discernible effect on the structure of myelinated axons or on the motor performance of the mutant animals. There were modest effects on both acute thermal and mechanical nociceptive behaviors and on the electrophysiological properties of sensory neurons. Without a direct experimental test, we cannot exclude the possibility that the lack of KCNQ2 in developing neurons contributes to the observed phenotype or that compensation may have diminished the effects of deleting *Kcnq2*.

Kv7.3 nodal expression does not depend on Kv7.2

Our data confirm that Kv7.2 and Kv7.3 are found at nodes (Devaux et al., 2004; Pan et al., 2006; Schwarz et al., 2006), although we document an even greater extent of their colocalization. This finding suggests that Kv7.2/Kv7.3 heteromers are the main Kv7 channels at PNS nodes. The localization of Kv7.3 at *Kcnq2*-null nodes demonstrates that Kv7.3 surface expression does not require Kv7.2, in contrast to previous in vitro studies (Schwake et al., 2000; Gomez-Posada et al., 2010). Because both Kv7.2 and Kv7.3 contain an

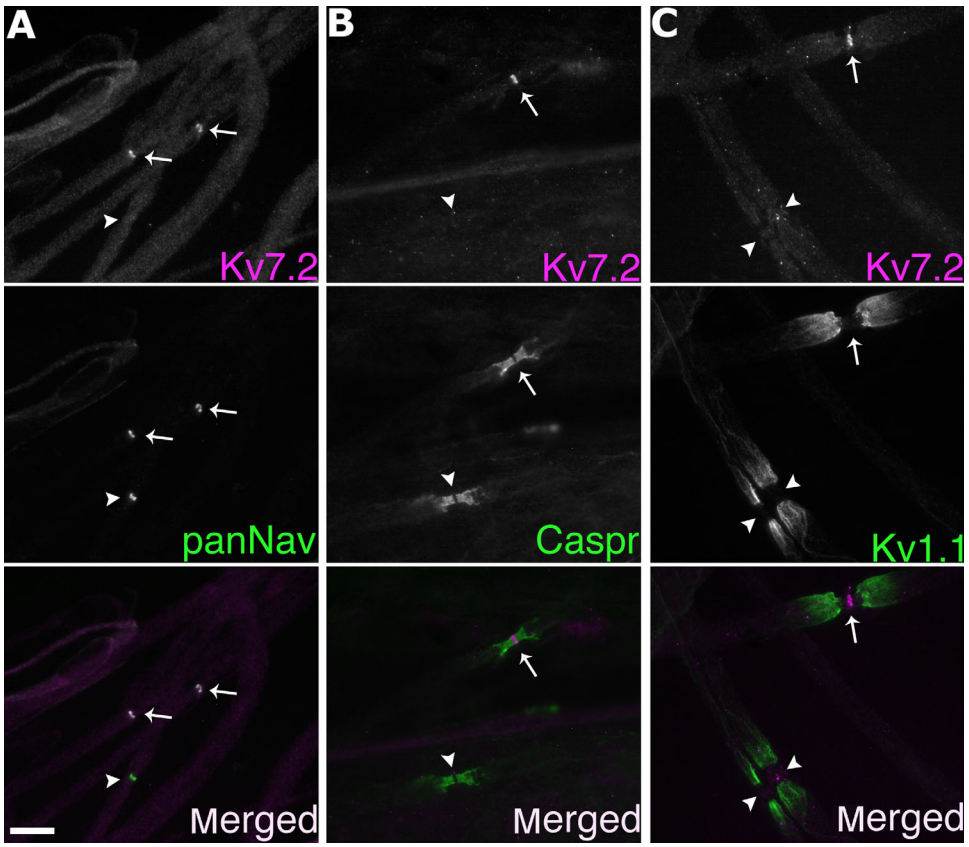

Figure 8. The molecular components of nodes, paranodes and juxtaparanodes are maintained in *Kcnq2*-null sensory axons. Digital images of teased fibers from unfixed mutant sciatic nerves, double labeled for Kv7.2 (magenta) and panNav (column A), Caspr (column B), or Kv1.1 (column C); all green. The selected nodal (panNav), paranodal (Caspr), and juxtaparanodal (Kv1.1) components are the same for myelinated axons with Kv7.2-positive (motor axons) or Kv7.2-negative (sensory axons) nodes. Scale bar = 10 μm.

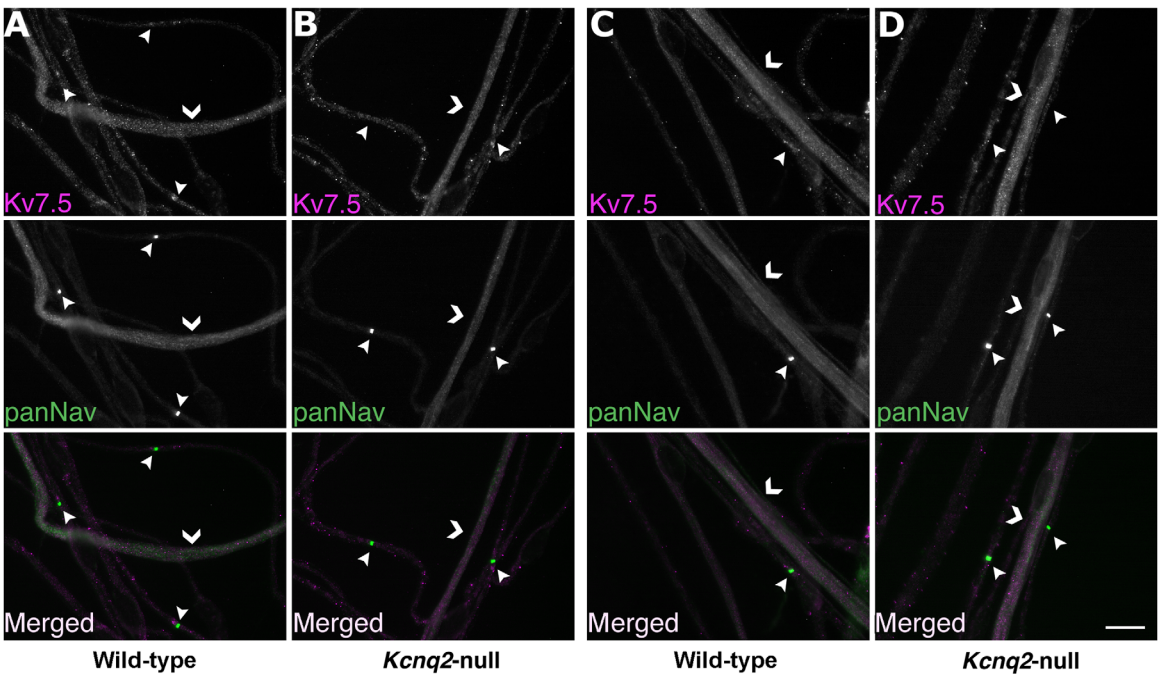

Figure 9. Remak fiber expression of Kv7.5 is maintained in *Kcnq2* mutant mice. Digital images of unfixed mouse teased nerves, double labeled for Kv7.5 (magenta) and panNav (green). In the femoral sensory (columns A and B) and motor (columns C and D) branches of both mutant and wild-type mice, all panNav-positive Remak fibers are Kv7.5 positive (chevrons), whereas all panNav-positive nodes are Kv7.5 negative (arrowheads). Scale bar = 10 μm.

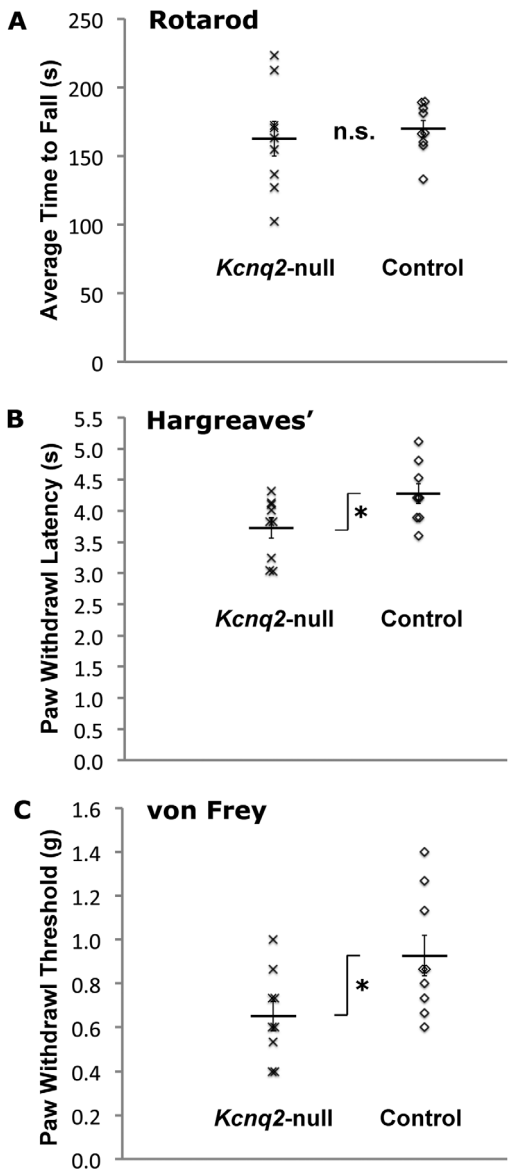

Figure 10. Behavioral testing of *Kcnq2*-null mice and control mice. **A:** Mutant mice (n = 9) and their control littermates (n = 9) were subjected to 3 consecutive days of testing on a rotarod (three tests per day), with motor performance measured by the time it took for the mice to fall off the rotarod. There was no statistical difference in the overall average time to fall between mutant and control animals. **B:** Both mutant mice (n = 9) and their control littermates (n = 9) were subjected to 4 consecutive days (six trials per day) of thermal hyperalgesia measured by the withdrawal latency after thermal stimulation (on a Hargreaves chamber). The overall average of all tests showed that mutant animals have a statistically significant increase in thermal hyperalgesia. **C:** Both mutant mice (n = 9) and control littermates (n = 9) were subjected to 3 consecutive days of testing with a series of von Frey hair filaments (0.4, 0.6, 1.0, 1.4, and 2.0 g; one up-and-down session per day). Mechanical allodynia was determined by the lowest strength of hair filament capable of inducing a positive withdrawal response. The overall average of all tests showed that mutant animals have a statistically significant increase in mechanical allodynia. For all three behavior tests, error bars represent SEM; n.s., no significant difference. $^*P < 0.05$ (unpaired two-sample Student's *t*-test with equal variance).

ankyrin-G binding domain (Pan et al., 2006), it is reasonable to expect that Kv7.3 could be selectively retained at nodes and AIS. Indeed, the deletion of the ankyrin-G binding motif in Kv7.2 alone does not alter the AIS localization of Kv7.2/Kv7.3 heteromers (Rasmussen et al., 2007). In addition, the normal molecular components of nodes (panNav), paranodes (Caspr), and juxtaparanodes (Kv1.1) and the ultrastructure of *Kcnq2*-null sensory myelinated axons show that these features do not depend on Kv7.2. Finally, we found that Kv7.5 expression in Remak bundles is maintained in *Kcnq2*-null nerves. Although Kv7.5 and Kv7.3 can form heteromeric channels in vitro (Schroeder et al., 2000), we did not detect Kv7.5 immunoreactivity at *Kcnq2*-null nodes, suggesting that in our mutant animals the nodal Kv7 channels are comprised of Kv7.3 homomers.

TABLE 2.

Passive and Active Membrane Properties of Control and *Kcnq2*-Null DRG Neurons[1]

	Control	*Kcnq2*-null
Passive properties		
C_m (pF)	39 ± 3.3	45 ± 4.1
Initial RMP (mV)	−58 ± 2.5	−56 ± 1.6
Predrug firing properties		
Fast AHP peak (mV)	−83 ± 1.3	−86 ± 0.97[2]
AP rheobase (nA)	0.77 ± 0.23	0.81 ± 0.16
1× Rheobase (No. APs)	2.1 ± 0.38	2.9 ± 0.75
2× Rheobase (No. APs)	5.8 ± 1.3	11 ± 2.8
3× Rheobase (No. APs)	8.0 ± 1.3	17. ± 4.4[2]
Absolute stimulus (No. APs)	16 ± 1.6	25 ± 5.2[2]
Slow AHP peak (mV)	−74 ± 1.9	−68 ± 1.2[3]
Postdrug firing properties		
Fast AHP peak (mV)	−82 ± 0.97	−84 ± 1.21
AP rheobase (nA)	0.39 ± 0.07	0.88 ± 0.19[2]
1× Rheobase (No. APs)	4.0 ± 1.1	2.5 ± 0.66
2× Rheobase (No. APs)	11 ± 2.0	9.2 ± 2.2
3× Rheobase (No. APs)	13 ± 2.2	16 ± 2.9
Absolute stimulus (No. APs)	21 ± 2.2	23 ± 3.9
Slow AHP peak (mV)	−66 ± 1.2	−67 ± 1.6

[1]Twenty-five DRG neurons from five animals were recorded in the control and *Kcnq2*-null groups. Values are means ± SEM. C_m, membrane capacitance; RMP, resting membrane potential; AHP, afterhyperpolarization potential; fast AHP peak, AHP undershoot peak magnitude after a single 3-ms stimulus; AP rheobase, either the minimum amount of current required to evoke a single AP or 0.1 nA (whichever was smallest); 1×, 2×, and 3× rheobase, the number of APs fired by a DRG neuron during a 500-ms depolarizing current step of a magnitude 1×, 2×, or 3× its rheobase, respectively; absolute, the maximum number of APs fired in response to a single 500-ms depolarizing current step of 0.1–0.9-nA magnitude (in 0.1-nA increments); slow AHP peak, AHP undershoot magnitude after 500-ms stimulus at 0.4 nA. Values of C_m of the control DRG neurons was compared with that mutant neurons using unpaired two-sample Student's *t*-test with equal variance; AHP and AP rheobase were compared with two-way ANOVA with Tukey test; numbers of APs were compared with two-way repeated-measures ANOVA.

[2]$P < 0.05$.

[3]$P < 0.01$.

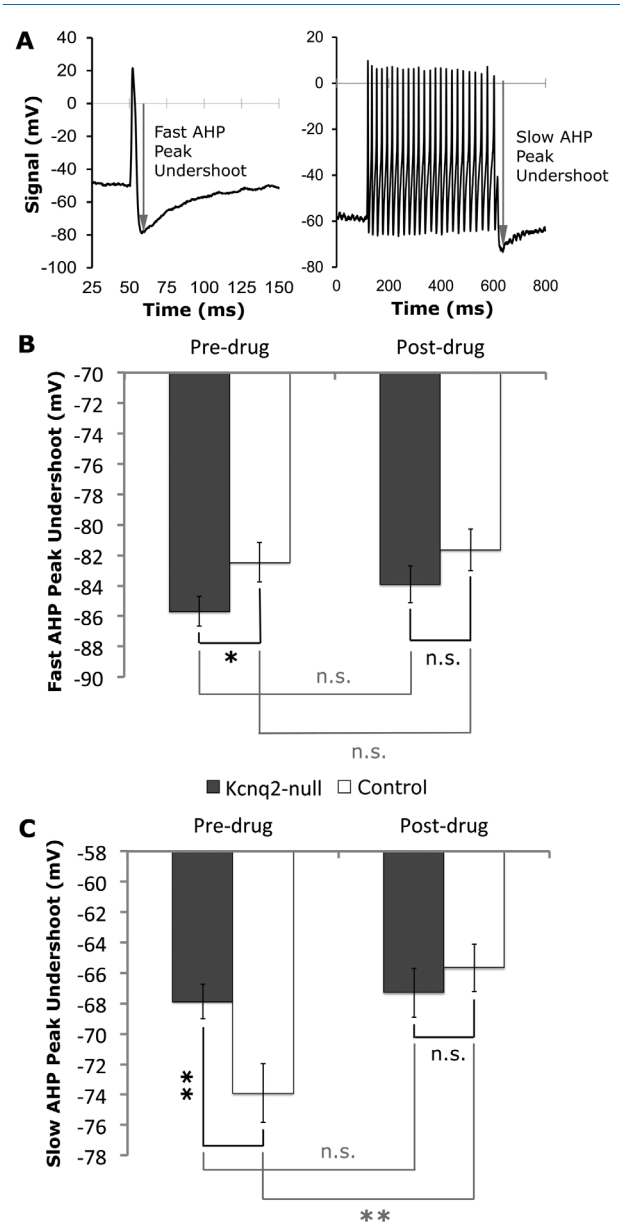

Figure 11. *Kcnq2*-null DRG neurons have a diminished slow afterhyperpolization (AHP) that is not affected by 3 mM TEA. **A** shows representative responses from a control DRG neuron given a brief (3 ms) depolarizing current step that generated a single action potential (AP) and a prolonged (500 ms) depolarizing current step that generated multiple APs, from which the magnitude of the fast and slow AHP peak undershoots, respectively, were measured. **B** shows that, before 3 mM TEA, the average fast AHP peak undershoot of mutant neurons (n = 25) was slightly more negative than that of control neurons (n = 25). After applying 3 mM TEA, the fast AHP peak undershoot of both control and *Kcnq2*-null neurons did not change by a statistically significant amount. **C** shows that, before 3 mM TEA, the average slow AHP peak undershoot of mutant neurons (n = 25) was 6 mV more positive than that of control neurons (n = 25). After applying 3 mM TEA for 2 minutes, the slow AHP peak undershoot of control neurons became 8 mV more positive, whereas the slow AHP peak undershoot of *Kcnq2*-null neurons did not change by a statistically significant amount. $*P < 0.05$, $**P < 0.01$ (two-way ANOVA).

Kv7.2 contributes to the regulation of neuronal excitability

Kv7 channels activate at subthreshold potentials and do not become inactivated, thereby contributing to the regulation of neuronal excitability (Brown and Passmore, 2009). Kv7 blockers (linopridine or XE991), dominant-negative Kv7.2 mutants, and decreased Kv7.2 expression have all been shown to increase excitability (decreased spike-frequency adaptation and/or increased number of action potentials) of hippocampal neurons (Aiken et al., 1995; Yue and Yaari, 2004; Gu et al., 2005; Peters et al., 2005; Shah et al., 2008) and of somatic and visceral sensory neurons (Passmore et al., 2003; Rivera-Arconada and Lopez-Garcia, 2005; Wladyka and Kunze, 2006; Wladyka et al., 2008; Zheng et al., 2013). A Kv7 enhancer (retigabine) produces the opposite effects (Lerche et al., 2000; Brueggemann et al., 2007). In isolated rat peripheral nerves, retigabine slows axonal conduction, and these effects can be reversed by application of linopridine or TEA (Devaux et al., 2004). Schwarz et al. (2006) showed that XE991 both abolishes the slow accommodation to the depolarization and the postdepolarization undershoot of action potential at nodes and increases repetitive firing and decreases spike-frequency adaptation in rat motor axons. Taken together, these results indicate that Kv7 channels regulate both neuronal and axonal activity.

Our analysis of *Kcnq2*-null DRG neurons confirms and extends these prior works. By using TEA at a Kv7.2-specific concentration (Wang et al., 1998; Hadley et al., 2000, 2003; Lerche et al., 2000), we show that Kv7.2 contributes to the spike-frequency adaptation of sensory neurons. Because TEA did not further decrease spike-frequency adaptation in *Kcnq2*-null neurons, decreased Kv7.2 activity is the most parsimonious explanation for the increased excitability of the *Kcnq2*-null neurons.

Classically, AHP can be subdivided into three phases, fast (1–5 ms), medium (50–200 ms), and slow (500 ms to several seconds) AHP (Madison and Nicoll, 1984; Storm, 1990; Gu et al., 2005). Because of the slow activation speed of the M-channels (tens of milliseconds), they do not contribute materially to the fast AHP (Brown and Passmore, 2009), which is instead considered to be mediated by the big potassium (BK) family of potassium channels (Storm, 1990). Indeed, our *Kcnq2*-null neurons exhibited only slightly more negative fast AHP amplitude compared with control neurons, and the application of TEA did not statistically change fast AHP amplitudes in either mutant or control neurons. The negative TEA results indicate that Kv7.2 does not play an appreciable role in the fast AHP. We cannot explain why the fast AHP amplitude of our *Kcnq2*-null neurons was slightly

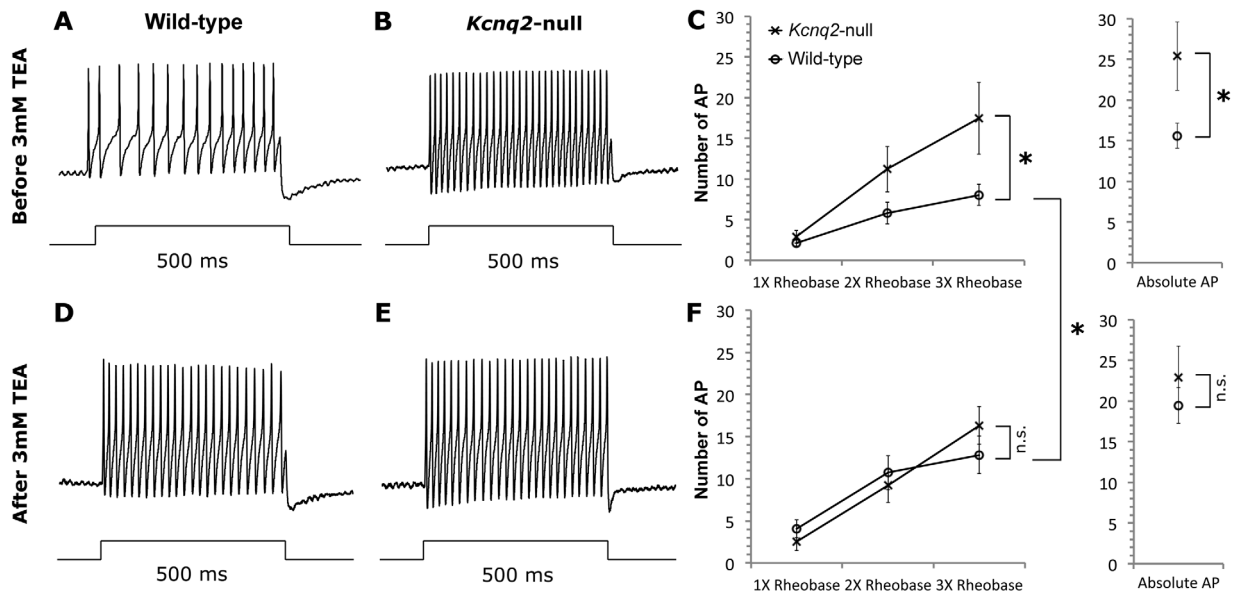

Figure 12. *Kcnq2*-null DRG neurons have decreased spike-frequency adaption that is not affected by 3 mM TEA. Single DRG neurons were injected with 500-ms depolarizing current steps of 1×, 2×, or 3× rheobase (**A–F**) from a holding level of between −50 and −60 mV before and after application of 3 mM TEA. Panels A–E show representative recordings of control (A,D) and mutant (B,E) neurons, before and after application of 3 mM TEA for 2 minutes. C and F are summary diagrams showing the number of APs in mutant and control neurons, before and after applying TEA, respectively (*$P < 0.05$; two-way repeated-measures ANOVA). Notably, after TEA application, control DRG neurons also showed a decrease in spike frequency adaption and generated statistically similar numbers of APs at each rheobase compared with mutant (n.s., no significant difference; two-way repeated-measures ANOVA). In contrast, TEA application did not reduce spike-frequency adaptation of the mutant DRG neurons. In addition, we also injected 500-ms incremental current at set current steps from 0.4 to 3.6 nA (in increments of 0.4 nA) to determine the responsiveness of DRG neurons to absolute (as opposed to relative threshold, as described above) depolarizing stimuli, and the spike frequency adaption was also significantly reduced in mutant DRG neurons in comparison with control neurons before TEA application; after TEA application, the control neurons generated statistically similar numbers of APs in response to absolute stimuli compared with mutant neurons.

more negative compared with the control neurons, but the fact that Kv7.2-specific concentration of TEA did not change the fast AHP amplitude of the control neurons suggests that this difference might not be due to the lack of Kv7.2 activity.

On the other hand, the identity of the channel(s) that mediates the slow AHP is still unclear, but decreases in Kv7.2 or Kv7.5 activity have been shown to reduce slow AHP in mouse hippocampal neurons (Tzingounis and Nicoll, 2008; Tzingounis et al., 2010). Our *Kcnq2*-null DRG neurons also displayed a decrease in slow AHP amplitude compared with control neurons, and 3 mM TEA was able to reduce the slow AHP amplitude of control neurons, while having no effect on mutant neurons. While a previous study has shown that 10 μM XE991 application in hippocampal neurons had actually enhanced slow AHP, other experiments showed that muscarine, which suppresses Kv7 channels (Brown and Adams, 1980), was able to inhibit slow AHP in the supraoptic neurons (Ghamari-Langroudi and Bourque, 2004; Hu and Mooney, 2005), which have also been shown to express Kv7 (Zhang et al., 2009). Therefore, although the exact contribution of Kv7 channels to slow AHP remains unclear, our results raise the possibility that Kv7.2 activity does contribute, at least in part, to slow AHP in DRG neurons.

Increased mechanical allodynia and thermal hyperalgesia in *Kcnq2*-null mice

The results regarding the role of Kv7 channels in mechanical allodynia and thermal hyperalgesia are inconsistent. In one study, retigabine increases the tail withdrawal threshold to noxious thermal stimuli in a dose-dependent manner (Dost et al., 2004), but because this effect was not reversed by the coadministration of linopridine, it may be due to a non-Kv7-specific effect of retigabine. This finding also conflicts with another study using different methodology, in which retigabine did not affect the withdrawal response from noxious thermal stimuli (Blackburn-Munro and Jensen, 2003). Similarly, intraplantar injections of XE991 into the rat hindpaws did not induce thermal hyperalgesia or mechanical allodynia (Linley et al., 2008). These

studies shared the important limitation that the enhancers and blockers likely act on most or all Kv7 subunits and potentially on other channels (for example, $GABA_A$; Otto et al., 2002). Unmyelinated axons express Kv7.5 (King and Scherer, 2012), which could also be the site of these pharmacological agents.

Our current study was designed to minimize these confounding factors by analyzing a type of myelinated sensory axons that lacks Kv7.2, the A-delta fibers. Although technical limitations do not allow us to completely differentiate A-delta fiber-mediated nociception from C fiber-mediated nociception, previous studies suggest that withdrawal reflex behavior from both acute noxious thermal stimuli (Price and Dubner, 1977; Dubner and Bennett, 1983; Yeomans and Proudfit, 1996; Hargreaves et al., 1998; Cuellar et al., 2010) and punctate mechanical stimuli (Dubner and Bennett, 1983; Koltzenburg et al., 1993; Ziegler et al., 1999) are both mediated primarily by A-delta fibers. Specifically, Yeomans and Proudfit (1996) found that radiant heating of rat hindpaw at a high rate of 6.5°C/second for 6 seconds evokes primarily an A-delta fiber response, whereas a low rate of 0.9°C/second for 20 seconds activates primarily a C fiber response; notably, the C fiber response at either heating rate did not begin until 5–8 seconds after onset of heating. Because the thermocouple of our Hargreaves apparatus had been shown to raise rat hindpaw temperature from 30°C to 49°C in 5 seconds (3.8°C/second; Dirig et al., 1997), and because the average withdrawal latencies of both mutant and control animals in our Hargreaves test were less than 5 seconds (3.7 and 4.3 seconds, respectively), our results suggest that the increased thermal hyperalgesia behavior of our *Kcnq2*-null mutant animal was, at least in part, due to increased A-delta fiber activity. Furthermore, Ji et al. (2007) reported that rats treated with spinal nerve ligation displayed decreased mechanical threshold of A-delta fibers, but not of C fibers, and simultaneously exhibited increased mechanical allodynia (as tested with von Frey filaments), suggesting that the increased mechanical allodynia of our *Kcnq2*-null animals might also be due to increase A-delta fiber activity. Finally, Passmore et al. (2012) showed that M-current inhibition by XE991 (at a concentration that is relatively selective against Kv7.2) enhanced the response of A-delta fibers, but not C fibers, to noxious heat stimulation. Taken together, the increased thermal hyperalgesia and mechanical allodynia exhibited by our *Kcnq2*-null mice suggest that the lack of Kv7.2 expression in the A-delta fibers may produce increased acute thermal and mechanical nociception. Because our rotarod test provided no evidence of different motor performance between the mutant and the control animals, the increased nociceptive responses observed in the *Kcnq2*-null mice is unlikely to be a consequence of altered motor behavior. However, because our X-gal stainings indicate that *Pax3-Cre* expression may also be present in regions of the brain, the possibility exists that the loss of Kv7.2 expression within the central nervous system also played a role in the increased thermal hyperalgesia and mechanical allodynia exhibited by our *Kcnq2* mutant mice.

Taken together, our work raises the possibility that decreasing Kv7.2 activity can increase sensory neuronal excitability, and lead to increased perception of mechanical and acute thermal pain.

ACKNOWLEDGMENTS

We like to thank Drs. Edward Cooper, Jérôme Devaux, and Virginia Lee for cDNAs and antisera; Dr. Gordon Barr for loaning us the Hargreaves apparatus; Dr. Ted Abel for loaning us the rotarod; Dr. Beth Winkelstein for advice regarding the von Frey hair filament test; Dr. Marc Dichter for the use of the electrophysiology rig; and Dr. Jian Li for help with the histology. Elior Peles is the Incumbent of the Hanna Hertz Professorial Chair for Multiple Sclerosis and Neuroscience.

CONFLICT OF INTEREST STATEMENT

The authors declare that they have no conflicts of interest.

ROLE OF AUTHORS

All authors had full access to all the data in the study and take responsibility for the integrity of the data and the accuracy of the data analysis. Study concept and design: CHK, EP, SSS. Acquisition of data: CHK, EL, DS. Analysis and interpretation of data: CHK, EL, DS, EP, SSS. Drafting of the manuscript: CHK, SSS. Critical revision of the manuscript for important intellectual content: CHK, EL, DS, EP, SSS. Statistical analysis: CHK. Obtained funding: EP, SSS. Administrative, technical, and material support: CHK, EL, DS, EP, SSS. Study supervision: EP, SSS.

LITERATURE CITED

Aiken SP, Lampe BJ, Murphy PA, Brown BS. 1995. Reduction of spike frequency adaption and blockade of M-crrent in rat CA1 pyramidal neurones by linopirdine (DuP 996), a neurotransmitter release enhancer. Br J Pharmacol 115: 1163–1168.

Arroyo EJ, Bermingham JRJ, Rosenfeld MG, Scherer SS. 1998. Promyelinating Schwann cells express Tst-1/SCIP/Oct-6. J Neurosci 18:7891–7902.

Blackburn-Munro G, Jensen BS. 2003. The anticonvulsant retigabine attenuates nociceptive behaviours in rat models of persistent and neuropathic pain. Eur J Pharmacol 460: 109–116.

Brown DA, Adams PR. 1980. Muscarinic suppression of a novel voltage sensitve K^+ current in a vertebrate neuron. Nature 283:673–676.

Brown DA, Passmore GM. 2009. Neural KCNQ (Kv7) channels. Br J Pharmacol 156:1185–1195.

Brueggemann LI, Moran CJ, Barakat JA, Yeh JZ, Cribbs LL, Byron KL. 2007. Vasopressin stimulates action potential firing by protein kinase C-dependent inhibition of KCNQ5 in A7r5 rat aortic smooth muscle cells. Am J Physiol Heart Circ Physiol 292:H1352–H1363.

Caminos E, Garcia-Pino E, Martinez-Galan JR, Juiz JM. 2007. The potassium channel KCNQ5/Kv7.5 is localized in synaptic endings of auditory brainstem nuclei of the rat. J Comp Neurol 503:363–378.

Chaplan SR, Bach FW, Pogrel JW, Chung JM, Yaksh TL. 1994. Quantitative assessment of tactile allodynia in the rat paw. J Neurosci Methods 53:55–63.

Cooper EC, Harrington E, Jan YN, Jan LY. 2001. M channel KCNQ2 subunits are localized to key sites for control of neuronal network oscillations and synchronization in mouse brain. J Neurosci 21:9529–9540.

Cuellar JM, Manering NA, Klukinov M, Nemenov MI, Yeomans DC. 2010. Thermal nociceptive properties of trigeminal afferent neurons in rats. Mol Pain 6:39.

Dedek K, Kunath B, Kananura C, Reuner U, Jentsch TJ, Steinlein OK. 2001. Myokymia and neonatal epilepsy caused by a mutation in the voltage sensor of the KCNQ2 K^+ channel. Proc Natl Acad Sci U S A 98: 12272–12277.

Delmas P, Brown DA. 2005. Pathways modulating neural KCNQ/M (Kv7) potassium channels. Nat Rev Neurosci 6: 850–862.

Devaux JJ, Kleopa KA, Cooper EC, Scherer SS. 2004. KCNQ2 is a nodal K^+ channel. J Neurosci 24:1236–1244.

Dirig DM, Salami A, Rathbun ML, Ozaki GT, Yaksh TL. 1997. Characterization of variables defining hindpaw withdrawl latency evoked by radiant thermal stimuli. J Neurosci Methods 76:183–191.

Dost R, Rostock A, Rundfeldt C. 2004. The anti-hyperalgesic activity of retigabine is mediated by KCNQ potassium channel activation. Naunyn-Schmiedebergs Arch Pharmacol 369:382–390.

Dubner R, Bennett GJ. 1983. Spinal and trigeminal mechanisms of nociception. Annu Rev Neurosci 6:381–418.

Farley FW, Soriano P, Steffen LS, Dymecki SM. 2000. Widespread recombinase expression using FLPeR (Flipper) mice. Genesis 28:106–110.

Feltri ML, Scherer SS, Wrabetz L, Kamholz J, Shy ME. 1992. Mitogen-expanded Schwann cells retain the capacity to myelinate regenerating axons after transplantation into rat sciatic nerve. Proc Natl Acad Sci U S A 89:8827–8831.

Ghamari-Langroudi M, Bourque CW. 2004. Muscarinic receptor modulation of slow afterhyperpolarization and phasic firing in rat supraoptic nucleus neurons. J Neurosci 24: 7718–7726.

Goldman AM, Glasscock E, Yoo J, Chen TT, Klassen TL, Noebels JL. 2009. Arrhythmia in heart and brain: KCNQ1 mutations link epilepsy and sudden unexplained death. Science Translational Med 1:2ra6.

Gollan L, Salomon D, Salzer JL, Peles E. 2003. Caspr regulates the processing of contactin and inhibits its binding to neurofascin. J Cell Biol 163:1213–1218.

Gomez-Posada JC, Etxeberria A, Roura-Ferrer M, Areso P, Masin M, Murrell-Lagnado RD, Villarroel A. 2010. A pore residue of the KCNQ3 potassium M-channel subunit controls surface expression. J Neurosci 30:9316–9323.

Gu N, Vervaeke K, Hu H, Storm JF. 2005. Kv7/KCNQ/M and HCN/h, but not KCa2/SK channels, contribute to the somatic medium after-hyperpolarization and excitability control in CA1 hippocampal pyramidal cells. J Physiol 566:689–715.

Hadley JK, Noda M, Selyanko AA, Wood IC, Abogadie FC, Brown DA. 2000. Differential tetraethylammonium sensitivity of KCNQ1–4 potassium channels. Br J Pharmacol 129:413–415.

Hadley JK, Passmore GM, Tatulian L, Al-Qatari M, Ye F, Wickenden AD, Brown DA. 2003. Stoichiometry of expressed KCNQ2/KCNQ3 potassium channels and subunit composition of native ganglionic M channels deduced from block by tetraethylammonium. J Neurosci 23:5012–5019.

Hamill OP, Marty A, Neher E, Sakmann B, Sigworth FJ. 1981. Improved patch-clamp techniques for high-resolution current recording from cells and cell free membrane patches. Pflugers Arch 391:85–100.

Hargreaves K, Dubner R, Brown F, Flores C, Joris J. 1988. A new and sensitive method for measuring thermal nociception in cutaneous hyperalgesia. Pain 32:77–88.

Hargreaves KM, Swift JQ, Roszkowski MT, Bowles W, Garry MG, Jackson DL. 1998. Pharmacology of peripheral neuropeptide and inflammatory mediator release. Oral Surg Oral Med Oral Pathol 78:503–510.

Heidenreich M, Lechner SG, Vardanyan V, Wetzel C, Cremers CW, De Leenheer EM, Aránguez G, Moreno-Pelayo MÁ, Jentsch TJ, Lewin GR. 2011. KCNQ4 K^+ channels tune mechanoreceptors for normal touch sensation in mouse and man. Nat Neurosci 15:138–145.

Hu B, Mooney DM. 2005. Burst firing induces a slow after hyperpolarization in rat auditory thalamus. Neurosci Lett 375:162–164.

Hubbard RD, Winkelstein BA. 2005. Transient cervical nerve root compression in the rat induces bilateral forepaw allodynia and spinal glial activation: mechanical factors in painful neck injuries. Spine 30:1924–1932.

Ikeda SR, Schofield GG, Weight FF. 1986. Na^+ and Ca^{2+} currents of acutely isolated adult rat nodose ganglion cells. J Neurophysiol 55:527–539.

Jentsch TJ. 2000. Neuronal KCNQ potassium channels: physiology and role in disease. Nat Rev Neurosci 1:21–30.

Ji G, Zhou S, Kochukov MY, Westlund KN, Carlton SM. 2007. Plasticity in intact A delta- and C-fibers contributes to cold hypersensitivity in neuropathic rats. Neuroscience 150:182–193.

King CH, Scherer SS. 2012. Kv7.5 is the primary Kv7 subunit expressed in C-fibers. J Comp Neurol 520:1940–1950.

Koltzenburg M, Lundberg LE, Torebjork HE. 1993. Dynamic and static components of mechanical hyperalgesia in human hairy skin. Pain 51:207–219.

Lancaster E, Oh EJ, Weinreich D. 2001. Vagotomy decreases excitability in primary vagal afferent somata. J Neurophysiol 85:247–253.

Lang PM, Fleckenstein J, Passmore GM, Brown DA, Grafe P. 2008. Retigabine reduces the excitability of unmyelinated peripheral human axons. Neuropharmacology 54: 1271–1278.

Lee KE, Davis MB, Winkelstein BA. 2008. Capsular ligament involvement in the development of mechanical hyperalgesia after facet joint loading: behavioral and inflammatory outcomes in a rodent model of pain. J Neurotrauma 25: 1383–1393.

Lerche C, Scherer CR, Seebohm G, Derst C, Wei AD, Busch AE, Steinmeyer K. 2000. Molecular cloning and functional expression of KCNQ5, a potassium channel subunit that may contribute to neuronal M-current diversity. J Biol Chem 275:22395–22400.

Li J, Chen F, Epstein JA. 2000. Neural crest expression of Cre recombinase directed by the proximal Pax3 promoter in transgenic mice. Genesis 26:162–164.

Linley JE, Rose K, Patil M, Robertson B, Akopian AN, Gamper N. 2008. Inhibition of M current in sensory neurons by exogenous proteases: a signaling pathway mediating inflammatory nociception. J Neurosci 28:11240–11249.

Madison DV, Nicoll RA. 1984. Control of the repetitive discharge of rat CA1 pyramidal neurons in vitro. J Physiol 354:319–331.

Malin SA, Davis BM, Molliver DC. 2007. Production of dissociated sensory neuron cultures and considerations for their use in studying neuronal function and plasticity. Nat Protoc 2:152–160.

Maljevic S, Lerche C, Seebohm G, Alekov AK, Busch AE, Lerche H. 2003. C-terminal interaction of KCNQ2 and KCNQ3 K^+ channels. J Physiol 548:353–360.

Nagy A. 2000. Cre recombinase: the universal reagent for genome tailoring. Genesis 26:99–109.

Ogawa Y, Oses-Prieto J, Kim MY, Horresh I, Peles E, Burlingame AL, Trimmer JS, Meijer D, Rasband MN. 2010. ADAM22, a Kv1 channel-interacting protein, recruits membrane-associated guanylate kinases to juxtaparanodes of myelinated axons. J Neurosci 30:1038–1048.

Oliveira AM, Abel T, Brindle PK, Wood MA. 2006. Differential role for CBP and p300 CREB-binding domain in motor skill learning. Behav Neurosci 120:724–729.

Otto JF, Kimball MM, Wilcox KS. 2002. Effects of the anticonvulsant retigabine on cultured cortical neurons: changes in electroresponsive properties and synaptic transmission. Mol Pharmacol 61:921–927.

Otto JF, Yang Y, Frankel WN, White HS, Wilcox KS. 2006. A spontaneous mutation involving *Kcnq2* (Kv7.2) reduces M-current density and spike frequency adaptation in mouse CA1 neurons. J Neurosci 26:2053–2059.

Pan Z, Kao T, Horvath Z, Lemos J, Sul JY, Cranstoun SD, Bennett V, Scherer SS, Cooper EC. 2006. A common ankyrin-G-based mechanism retains KCNQ and NaV channels at electrically active domains of the axon. J Neurosci 26:2599–2613.

Passmore GM, Selyanko AA, Mistry M, Al-Qatari M, Marsh SJ, Matthews EA, Dickenson AH, Brown TA, Burbidge SA, Main M, Brown DA. 2003. KCNQ/M currents in sensory neurons: significance for pain therapy. J Neurosci 23: 7227–7236.

Peles E, Nativ M, Lustig M, Grumet M, Schilling J, Martinez R, Plowman GD, Schlessinger J. 1997. Identification of a novel contactin-associated transmembrane receptor with multiple domains implicated in protein–protein interactions. EMBO J 16:978–988.

Peters HC, Hu H, Pongs O, Storm JF, Isbrandt D. 2005. Conditional transgenic suppression of M channels in mouse brain reveals functions in neuronal excitability, resonance and behavior. Nat Neurosci 8:51–60.

Poliak S, Gollan L, Martinez R, Custer A, Einheber S, Salzer JL, Trimmer JS, Shrager P, Peles E. 1999. Caspr2, a new member of the neurexin superfamily, is localized at the juxtaparanodes of myelinated axons and associated with K^+ channels. Neuron 24:1037–1047.

Poliak S, Salomon D, Elhanany H, Sabanay H, Kiernan B, Pevny L, Stewart CL, Xu X, Chiu SY, Shrager P, Furley AJ, Peles E. 2003. Juxtaparanodal clustering of Shaker-like K^+ channels in myelinated axons depends on Caspr2 and TAG-1. J Cell Biol 162:1149–1160.

Price DD, Dubner R. 1977. Mechanisms of first and second pain in the peripheral and central nervous systems. J Invest Dermatol 69:167–171.

Quinn KP, Dong L, Golder FJ, Winkelstein BA. 2010. Neuronal hyperexcitability in the dorsal horn after painful facet joint injury. Pain 151:414–421.

Rasband, MN, Trimmer JS, Schwarz TL, Levinson SR, Ellisman MH, Schachner M, Shrager P. 1998. Potassium channel distribution, clustering, and function in remyelinating rat axons. J Neurosci 18:36–47.

Rasband MN, Peles E, Trimmer JS, Levinson SR, Lux SE, Shrager P. 1999. Dependence of nodal sodium channel clustering on paranodal axoglial contact in the developing CNS. J Neurosci 19:756–7528.

Rasband MN, Park EW, Vanderah TW, Lai J, Porreca F, Trimmer JS. 2001. Distinct potassium channels on pain-sensing neurons. Proc Natl Acad Sci U S A 98:13373–13378.

Rasmussen HB, Frokjaer-Jensen C, Jensen CS, Jensen HS, Jorgensen NK, Misonou H, Trimmer JS, Olesen SP, Schmitt N. 2007. Requirement of subunit co-assembly and ankyrin-G for M-channel localization at the axon initial segment. J Cell Sci 120:953–963.

Rivera-Arconada I, Lopez-Garcia JA. 2005. Effects of M-current modulators on the excitability of immature rat spinal sensory and motor neurones. Eur J Neurosci 22:3091–3098.

Rivera-Arconada I, Lopez-Garcia JA. 2006. Retigabine-induced population primary afferent hyperpolarisation in vitro. Neuropharmacology 51:756–763.

Roza C, Lopez-Garcia JA. 2008. Retigabine, the specific KCNQ channel opener, blocks ectopic discharges in axotomized sensory fibres. Pain 138:537–545.

Sauer B, Henderson N. 1988. Site-specific DNA recombination in mammalian cells by the Cre recombinase of bacteriophage P1. Proc Natl Acad Sci U S A 85:5166–5170.

Schmalbruch H. 1986. Fiber composition of the rat sciatic nerve. Anat Rec 215:71–81.

Schroeder BC, Hechenberger M, Weinreich F, Kubisch C, Jentsch TJ. 2000. KCNQ5, a novel potassium channel broadly expressed in brain, mediates M-type currents. J Biol Chem 275:24089–24095.

Schwake M, Pusch M, Kharkovets T, Jentsch TJ. 2000. Surface expression and single channel properties of KCNQ2/KCNQ3, M-type K^+ channels involved in epilepsy. J Biol Chem 275:13343–13348.

Schwarz JR, Glassmeier G, Cooper EC, Kao TC, Nodera H, Tabuena D, Kaji R, Bostock H. 2006. KCNQ channels mediate IKs, a slow K^+ current regulating excitability in the rat node of Ranvier. J Physiol 573:17–34.

Selyanko A, Hadley JK, Brown DA. 2001. Properties of single M-type KCNQ2/KCNQ3 potassium channels expressed in mammalian cells. J Physiol 534:15–24.

Shah MM, Mistry M, Marsh SJ, Brown DA, Delmas P. 2002. Molecular correlates of the M-current in cultured rat hippocampal neurons. J Physiol 544:29–37.

Shah MM, Migliore M, Valencia I, Cooper EC, Brown DA. 2008. Functional significance of axonal Kv7 channels in hippocampal pyramidal neurons. Proc Natl Acad Sci U S A 105:7869–7874.

Singh NA, Charlier C, Stauffer D, Dupont BR, Leach RJ, Melis R, Ronen GM, Bjerre I, Quattlebaum T, Murphy JV. 1998. A novel potassium channel gene, KCNQ2, is mutated in an inherited epilepsy of newborns. Nat Genet 18:25–29.

Soriano P. 1999. Generalized lacZ expression with the ROSA26 Cre reporter strain. Nat Genet 21:70–71.

Storm JF. 1990. Potassium currents in hippocampal pyramidal cells. Prog Brain Res 83:161–187.

Tzingounis AV, Nicoll RA. 2008. Contribution of KCNQ2 and KCNQ3 to the medium and slow afterhyperpolarization currents. Proc Natl Acad Sci U S A 105:19974–19979.

Tzingounis AV, Heidenreich M, Kharkovets T, Spitzmaul G, Jensen HS, Nicoll RA, Jentsch TJ. 2010. The KCNQ5 potassium channel mediates a component of the

afterhyperpolarization current in mouse hippocampus. Proc Natl Acad Sci U S A 107:10232–10237.

Wang HS, Pan Z, Shi W, Brown BS, Wymore RS, Cohen IS, Dixon JE, MckKinnon D. 1998. KCNQ2 and KCNQ3 potassium channel subunits: molecular correlates of the M-channel. Science 282:1890–1893.

Watanabe H, Nagata E, Kosakai A, Nakamura M, Yokoyama M, Tanaka K, Sasai H. 2000. Disruption of the epilepsy KCNQ2 gene results in neural hyperexcitability. J Neurochem 75:28–33.

Wen H, Levitan IB. 2002. Calmodulin is an auxiliary subunit of KCNQ2/3 potassium channels. J Neurosci 22:7991–8001.

Wladyka CL, Kunze DL. 2006. KCNQ/M-currents contribute to the resting membrane potential in rat visceral sensory neurons. J Physiol 575:175–189.

Wladyka CL, Feng B, Glazebrook PA, Schild JH, Kunze DL. 2008. The KCNQ/M-current modulates arterial baroreceptor function at the sensory terminal in rats. J Physiol 586:795–802.

Wood MA, Kaplan MP, Park A, Blanchard EJ, Oliveira AM, Lombardi TL, Abel T. 2005. Transgenic mice expressing a truncated form of CREB-binding protein (CBP) exhibit deficits in hippocampal synaptic plasticity and memory storage. Learn Mem 12:111–119.

Yang Y, Beyer BJ, Otto JF, O'Brien TP, Letts VA, White HS, Frankel WN. 2003. Spontaneous deletion of epilepsy gene orthologs in a mutant mouse with a low electroconvulsive threshold. Hum Mol Genet 12:975–984.

Yeomans DC, Proudfit HK. 1996. Nociceptive responses to high and low rates of noxious cutaneous heating are mediated by different nociceptors in the rat: electrophysiological evidence. Pain 68:141–150.

Yue C, Yaari Y. 2004. KCNQ/M channels control spike afterdepolarization and burst generation in hippocampal neurons. J Neurosci 24:4614–4624.

Zheng QF, Liu M, Cai J, Wan Y, Han J-S, Xing G-G. 2013. Suppression of KCNQ/M (Kv7) potassium channels in dorsal root ganglion neurons contributes to the development of bone cancer pain in a rat model. Pain 154:434–448.

Ziegler EA, Mageri W, Meyer RA, Treede RD. 1999. Secondary hyperalgesia to punctate mechanical stimuli: central sensitization to A-fibre nociceptor input. Brain 122:2245–2257.